Quasielastic scattering of pions from ^{16}O at energies around the $\Delta(1232)$ resonance

C. H. Q. Ingram
Schweizerisches Institut für Nuklearforschung, CH-5234, Villigen, Switzerland
and Kernforschungszentrum, Institut für Kernphysik
und Institut für Experimentelle Kernphysik der Universität,
D-7500 Karlsruhe, Federal Republic of Germany

P. A. M. Gram,* J. Jansen, R. E. Mischke,* and J. Zichy
Schweizerisches Institut für Nuklearforschung, CH-5234, Villigen, Switzerland

J. Bolger, E. T. Boschitz, and G. Pröbstle
Kernforschungszentrum, Institut für Kernphysik
und Institut für Experimentelle Kernphysik der Universität,
D-7500, Karlsruhe, Federal Republic of Germany

J. Arvieux†
Institut des Sciences Nucléaires, Université de Grenoble, F-38044, Grenoble, France
(Received 23 August 1982)

Inelastic pion scattering from ^{16}O has been studied by measuring the spectrum of pions down to 40 MeV at five angles between 30° and 134° for three incident pion energies: 114, 163, and 240 MeV. The spectra are dominated by a broad peak due to quasielastic scattering from a single nucleon in the nucleus. The systematics of the spectra are discussed with emphasis on the pion-nucleus interaction dynamics including the effect of absorption. The partial π^+-^{16}O cross sections for all nonradiative channels are estimated.

[NUCLEAR REACTIONS $^{16}O(\pi,\pi')$ $E=114$, 163, 240 MeV. $\theta=30-134°$, full inelastic spectrum measured; $\sigma(\theta)$. Discussion of nuclear medium effects on quasifree processes, Δ propagation.]

I. INTRODUCTION

The pion-nucleon interaction in the energy range 100–300 MeV is dominated by the $\Delta(1232)$, the strongest of the meson-nucleon resonances. The interaction, and hence the resonance, is affected by the presence of other nucleons when the target nucleon is bound in a nucleus. One modification to the free scattering amplitude is that due to pion absorption, which cannot occur on a free nucleon, but which is an important contributor to the pion-nuclear inelasticity. Studying pion-nucleus interactions thus allows an investigation of the behavior of a strong resonance in nuclear matter and also a study of the dynamics of pion absorption, which will advance our understanding of the nuclear force.

While the dominance of the Δ resonance and the large pion absorption probability indicate that we should be able to study them in nuclei in some detail, the complexities of nuclear interactions are such that these studies are not straightforward and require careful theoretical interpretation of experimental data. To have confidence that theory has correctly associated aspects of the data with the phenomena of interest, it is necessary to have a comprehensive experimental knowledge of the major pion-nucleus interaction channels, reproduced or accommodated by the theory in a consistent way. Theoretical models that are appropriate for investigating the pion- and Δ-nucleus dynamics are being developed.[1]

Much of the necessary experimental knowledge of pion-nucleus interactions is the result of recent work. Total and partial cross sections for pions on a range of nuclei at energies through the resonance region have been published.[2–6] Elastic scattering at these energies has been extensively studied,[7] but the reaction channels, comprising about 60% of the total cross section, are less well known even though they may be expected to give greater qualitative insight into the reaction dynamics. The two main parts of the reaction cross section are pion absorp-

tion and inelastic scattering to the continuum. Pion absorption is hard to study in a comprehensive way because the large energy deposit opens many possible final state channels. Inclusive measurements of the emitted proton spectra in (π,p) reactions[8] have been made that provide a valuable systematic overview of this part of the absorption reaction; however, the interpretation of these spectra is complicated by the uncertain multiplicity of the emitted nucleons and because some of the lower energy protons come from nonabsorptive reactions.

The experiment reported here, which measures the full spectrum of inelastic pions scattered in the $^{16}O(\pi,\pi')$ reaction, provides an inclusive overview of the inelastic part of the reaction cross section on one nucleus. In this reaction, there is only one pion in the final state (apart from a negligible contribution from pion-production reactions) whose origin is thus unambiguous. While these noncoincident pion spectrum measurements do not specify the final state of the nucleus and knocked-out nucleons, neither do they restrict them; and they have the merit that they cover the entire kinematic region down to a low-energy cutoff. This combination of completeness and lack of ambiguity concerning the processes involved is an important assistance to the qualitative interpretation of the inelastic pion spectra and, as will be seen, also allows quantitative comparison with theoretical models. Features of the spectra are sensitive to details of the pion-nucleus, and thus the Δ-nucleus reaction dynamics, while the completeness of the data helps to ascertain the nature of the balance between the absorption and inelastic reaction channels.

We present measurements of the energy spectra of π^+ scattered from ^{16}O for 114, 163, and 240 MeV incident energies at angles from 30° to 134°, covering the scattered pions's energy spectra down to 40 MeV. Preliminary results were reported in Ref. 7. Previous experiments of a nature similar to this one have either been more limited in scope,[9–11] or have lacked energy information on the scattered pion.[6,8] Early experiments[9,10] were hard to reconcile with each other or with other data.[12] Part of these problems may have been inadequate control of muon backgrounds in the continuum. The pion fluxes and instrumentation now available enabled this experiment to overcome these problems, although the elimination of backgrounds remains an important part of the data reduction necessary to produce reliable cross sections in the continuum region. An experiment similar in concept to this but exploring the single-charge-exchange (SCX) reaction,[13] which we would expect to reflect very similar physical processes, has been performed at 50 and 100 MeV.

The experiment is described in Sec. II and the data analysis in Sec. III. A discussion of what we have learned of the reaction dynamics accompanies the presentation of the results in Sec. IV, and the conclusions appear in Sec. V.

II. THE EXPERIMENT

The experiment was performed with the high-resolution pion channel and spectrometer[14] of the Schweizerisches Institut für Nuklearforschung (SIN). The standard layout of the installation is shown in Fig. 1, and a summary of its important characteristics for this experiment is given in Table I. Before starting this experiment, two 2-m-long multiwire proportional chambers with individual wire readout ($C6$ and $C7$ in Fig. 1), were installed near the spectrometer's focal plane, replacing the 1-m-long chambers described in Ref. 14. Each of these new chambers had an x plane of wires 2 mm apart (in the dispersive direction), and a u plane of

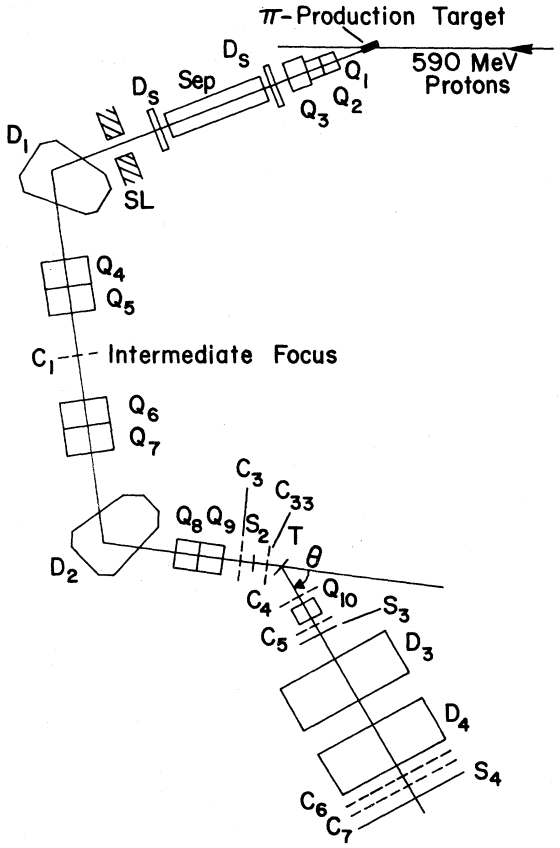

FIG. 1. Schematic view of the $\pi M1$ beam line ($Q1$ to T) and pion spectrometer (T to $S4$). Q=quadrupole magnet, D=dipole magnet, Sep=electrostatic separator, SL=adjustable slit, C=multiwire proportional chamber, S=plastic scintillator, T=scattering target.

TABLE I. Specifications of pion channel and spectrometer, as used in this experiment.

	Pion channel	Pion spectrometer
Solid angle	7 msr	11 msr
Momentum acceptance	±1.4%	±10%
Focal plane inclination	90°	35°
Dispersion (along focal plane)	7 cm/%	5.5 cm/%
Dispersion plane	horizontal	vertical
Axial magnification		6.5
Total path length	20.6 m	8.3 m
Spot size at scattering target	12 mm horizontal 9 mm vertical	
Angular divergence at scattering target	35 mrad horizontal 100 mrad vertical	
Angular acceptance		10°
Energy resolution in this experiment	1–2 MeV	

wires 2 mm apart at 30° to the x plane. The wire chambers immediately upstream of the target ($C3$ and $C33$) were only used to align the beam on the target. Two other wire chambers, $C4$ and $C5$, measured the trajectories of scattered particles at the entrance of the spectrometer.

The method of data taking was substantially as described elsewhere.[15] The incident beam of 2 to 5×10^6 π^+/s was counted in a 1-mm-thick scintillator ($S2$) covering the whole pion beam, 50 cm upstream of the target. The few protons not eliminated by the electrostatic separator[14] in the beam line were discarded by pulse-height analysis of the signals from $S2$. Momentum-analyzed muons and positrons in the beam were of negligible quantity ($<1\%$ of pions) at 163 and 240 MeV and were eliminated from the data by time-of-flight (TOF) measurement at 114 MeV, using the 50-MHz radiofrequency (rf) signal from the cyclotron as a strobe to compare to the $S2$ signal. The TOF path from the pion production target to $S2$ was 20 m. Muons from pion decay near $S2$ could not be eliminated; estimates by a Monte Carlo calculation suggested their number to be 5% to 10% of the pion flux; the proportion was assumed to stay constant for a given incident energy.

A water target, 200 mm wide$\times$100 mm high$\times$15 mm thick, with 50-μm Mylar walls, was used. The plane of the target was rotated to achieve standard transmission geometry for scattering angles less than 90° and reflection geometry for backward scattering angles. For data including the ^{16}O elastic scattering peak, the target was also used in transmission geometry for scattering angles greater than 90° in order to retain sufficient energy resolution to resolve the elastic and discrete inelastic peaks.

Some data were taken using BeO and Be targets, to confirm that the large π^+-p elastic scattering peak from the hydrogen in the water target did not cause unexpectedly large backgrounds in the ^{16}O inelastic spectrum and to assist in determining the structure of the ^{16}O background under the π^+-p peak at forward angles. A limited number of empty-target runs were also taken under a variety of conditions which demonstrated that these backgrounds were $\lesssim1\%$.

For each spectrometer and target angle, the incident beam was adjusted so that the spot at the target was at the center of acceptance of the spectrometer, to an accuracy of ±1 mm. This was necessary to compensate for small misalignments of the incident beam or of the target with the spectrometer rotation point, which moved the beam spot away from the narrow region of uniform acceptance. The adjustments required were typically $\sim0.05\%$ in the field of the second beam-line dipole magnet, moving the spot by ~5 mm perpendicular to the bend plane of the spectrometer. This adjustment could cause a maximum change in solid angle of $<1\%$ and in incident momentum of $<0.1\%$.

An event in the spectrometer was defined by a coincidence between the two scintillators $S3$ (200×200×1 mm) and $S4$ (2000×200×10 mm) (see Fig. 1). A coincidence between ($S3\cdot S4$) and ($S2\cdot\overline{S2_{\rm big}}\cdot$rf) defined a scattering event, where $\overline{S2_{\rm big}}$ is the absence of a large signal in $S2$ that could have been an incident proton. This caused an interrupt signal to be sent to a PDP-11/45 computer, which

then read out the data for that event from CAMAC-based electronics and stored them on magnetic tape. Data for each event consisted of wire-chamber information, time information for all scintillators, and pulse-height information for $S2$ and $S3$.

Scalers registering the important information (rates in scintillators, instantaneous beam rates, events, accidental coincidences, etc.) were read and the information was stored on magnetic tape by the computer periodically during data taking. Similarly, the currents in all magnets were monitored by the computer to verify their stability. The dipole magnet fields, giving the incident and scattered pions's momenta, were determined from a nuclear magnetic resonance frequency. On-line analysis of a large sample of the data monitored the efficiency of the multiwire chambers and allowed verification of the proper adjustment of experimental parameters such as the incident beam alignment.

Data were recorded at five scattering angles between 30° and 134° for each of the incident pion energies of 114, 163, and 240 MeV. The spectrum of scattered pions at each angle was measured in about eight steps of spectrometer central momentum, 10% apart, from the ^{16}O elastic peak to the lowest outgoing energy of about 40 MeV. The momentum steps were generally ordered to go from one end of the range to the other in 20% jumps, and then to return to the initial value at settings in between, to provide a short-term consistency check in the data. With a useful acceptance of the spectrometer of nearly 20% in momentum, almost every part of the spectrum was measured twice by these overlapping steps. An overall statistical accuracy of about 10% per 1-MeV bin was attained.

III. DATA ANALYSIS

The double differential cross section was derived from the data according to the following expression (apart from corrections for systematic errors discussed below):

$$\frac{d^2\sigma}{d\Omega\, dE} = \frac{N_s(\Delta E)}{N_i} \frac{1}{d\omega} \frac{1}{\Delta E} \frac{1}{t} \frac{1}{\eta_\pi} \frac{1}{\eta_0} , \qquad (1)$$

where N_s is the number of scattered pions recorded per unit energy loss, ΔE; N_i is the number of incident pions; $d\omega$ is the solid angle of the spectrometer; t is the target thickness in ^{16}O nuclei/cm^2; η_π is the fraction of scattered pions not decaying before the end of the spectrometer; and η_0 is the fraction of events analyzed (not lost to computer dead time and where all necessary wire chambers recorded a single track, for example).

The overall normalization was determined from the π^+-p elastic scattering, measured at each angle and compared to published phase shifts.[16] This accounted for effects such as muons counted in the incident beam, and target-thickness and solid-angle uncertainties.

In the measurement of a continuum spectrum, background contaminations can arise that are not immediately observed. Thus, a substantial part of the data-analysis effort was devoted to ensuring that the results were background-free. Determination of the variation of the spectrometer's effective solid angle with absolute momentum required great care. Evaluation of the efficiencies of the wire chambers was also an important aspect of the analysis. We shall discuss these and other points of the data analysis in turn.

A. Backgrounds

As mentioned previously, target-empty backgrounds were negligible. Accidental coincidences were monitored by delayed coincidences and were always $<1\%$ of the true coincidences. Other identified sources of background were muons and positrons from the decay of scattered pions and any events which were caused by scattered pions not passing directly through the spectrometer (e.g., particles which scatter from magnet pole faces). These backgrounds were often substantial and occasionally even greater than the signal. They were eliminated after examination of each particle's trajectory and TOF through the spectrometer.

Trajectory analysis, operating in the dispersive plane only, predicted the angle of the pion leaving the spectrometer from its coordinates at $C4$ and $C5$, with small momentum-dependent corrections. The predicted angle was then compared to the angle measured by $C6$ and $C7$ and the difference was recorded in a histogram. Figure 2 shows typical histograms of this quantity for high and low pion momenta. The width of the central peak was determined by multiple scattering in the material at the entrance and exit of the spectrometer. Care was taken that the trajectory analysis was equally good and equivalent for the full momentum acceptance of the spectrometer. Events showing a deviation greater than ± 35 mrad were rejected, these being typically $\sim 20\%$ of the events. Primarily these rejected events are muons from pions decaying in the spectrometer, especially in the last 2 to 3 m before $C7$. Most background from random coincidences and pions scattering from material in the spectrometer is eliminated by this criterion as well.

The limits of ± 35 mrad on the trajectory analysis were chosen to define the good-event peak at the lowest momentum. The same limits were used at all

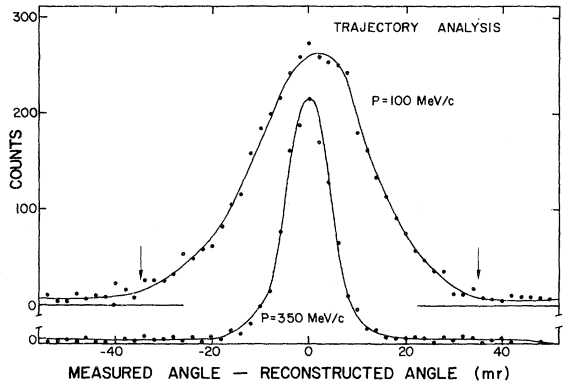

FIG. 2. Plots of the difference between the measured angle at the exit of the spectrometer and the angle predicted from the coordinates of the trajectory at the entrance, for two momenta. The limits between which events were accepted are indicated by the vertical arrows.

momenta for simplicity of analysis. Monte Carlo estimates indicated that typically $<3\%$ of events thus accepted were actually muons arriving at the momentum-defining chamber *C*6, giving an error on their parent pion's momentum determination in the spectrometer of $<4\%$. The wrongly determined momentum of such events yields a small but lengthy tail in the resolution function of the spectrometer, which generally was not significant for these data. The effect of a momentum dependence of the efficiency of the trajectory analysis was included in the analysis of the effective solid angle (see Sec. III B).

As a check of the validity of this procedure, the ratio of events accepted in a ± 17.5-mrad cut to those in the normal ± 35-mrad cut was recorded for all data. In particular, there was concern that a non-negligible background might arise in the vicinity of the very large π^+-p elastic peak. For almost all angles, this ratio varied systematically from 60% at 100 MeV/*c* to 95% at 330 MeV/*c*, with statistically insignificant variations. However, at 30° and 35°, and at 60° for 240-MeV incident pions, a local reduction in the ratio of 5% to 10% at momenta 8% below the elastic peak indicated a local change in the background. Based on this analysis, corrections of up to 20% (with up to 10% error) were applied to these regions of the forward-angle data.

The TOF through the spectrometer was also of great assistance for background rejection. This was measured by the time interval between a pulse defined by the logic rf·*S*2 and a pulse from *S*4. The path length through the spectrometer was determined from the wire-chamber coordinates. Resolution of 1.0 ns full width at half maximum (FWHM) was achieved over an average path length of 8 m. This was generally adequate to resolve pions from muons and positrons. Figure 3 shows TOF spectra at 135 and 280 MeV/*c*.

The spectra in Fig. 3 are constructed after the trajectory analysis cuts have been applied, implying that these muons and positrons are created before entering the spectrometer, i.e., they are the result of pions which scatter from the target and immediately decay. This background was present at all momenta, becoming substantial, typically $\sim 20\%$, below 200 MeV/*c*, and at forward angles sometimes becoming larger than the pion signal. However, it was always possible to put a satisfactory cut on the TOF spectrum, with a maximum error on the number of accepted events of $<\pm 3\%$.

In summary, the combination of trajectory and TOF analysis results in confidence that backgrounds are eliminated from the data. For the data in the region of the π^+-p elastic peak, there remain minor residual uncertainties for scattered pion energies up

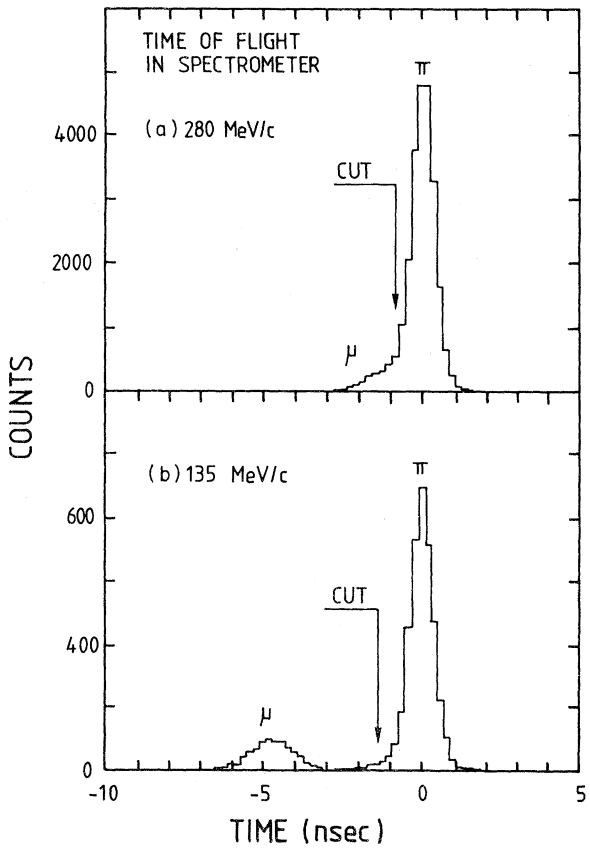

FIG. 3. Time of flight up to the end of the spectrometer for central momenta of (a) 280 MeV/*c* and (b) 135 MeV/*c*. Only events passing the trajectory analysis of Fig. 2 are included. At high momenta the fraction of muons was always small, but they were not well resolved and a tight cut was applied, for which a correction was applied to the data.

to 30 MeV below the π^+-p peak. These exceed 5% only at the most forward angles. They are included in the systematic errors in the results.

B. Solid angle of the spectrometer

The momentum acceptance $\Delta p/p$ of the spectrometer observed without restriction on the incident phase space is 35% FWHM and 20% full width at 90% of maximum. To simplify the analysis of these data, the angular acceptance of the spectrometer in the dispersive plane was restricted, reducing the solid angle from 16 to 11 msr. This enhanced the region of uniform momentum acceptance so that a range of 20% in $\Delta p/p$ could be used without correction. A maximum deviation from full transmission of $<5\%$ was tolerated.

The incident beam had a distribution 3% wide in momentum. Since cross sections are determined as functions of energy loss, this reduces the momentum acceptance of the system by 3% compared to the spectrometer's momentum acceptance, if the central momentum is that of the incident beam. For lower spectrometer momentum settings, the incident beam width, which is constant in MeV/c for a given incident energy, covers a larger fraction of the spectrometer's acceptance, so that the energy-loss acceptance was appropriately reduced.

The acceptance of the spectrometer for particles leaving a plane perpendicular to its axis, at the target position, is plotted in Fig. 4 as a function of horizontal displacement. This acceptance may be characterized as approximately Gaussian with a 35-mm FWHM, and a width of about 20 mm at 90% of maximum. For comparison, the incident beam had a natural width of about 15-mm FWHM and 25 mm at 5% of maximum. As seen by the spectrometer, this width is added to that of the 15-mm-wide target, which is itself also effectively enlarged according to the spectrometer and target angles. It is clear that the adjustment of the beam spot relative to the spectrometer's acceptance is of importance, and a sensitivity of about 2% per mm misadjustment was determined for these conditions. Alignment errors were usually <1 mm after proper adjustment, and the maximum correction applied to the data is 3% for this effect.

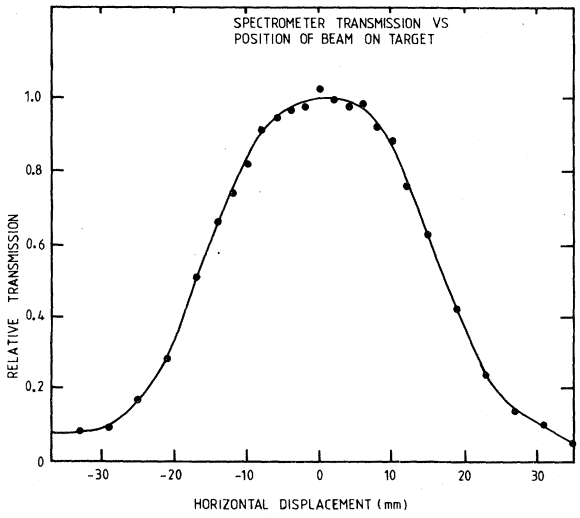

FIG. 4. Relative transmission of the spectrometer as a function of the horizontal displacement at a plane at the scattering target perpendicular to the spectrometer axis.

The shape of the acceptance curve (Fig. 4) is determined by three properties of the spectrometer: (1) The first-order magnification from the target to $S4$ is 6.5, which determines the rather narrow FWHM of 35 mm for the acceptance at the target. (2) Second-order optical effects ensure that the acceptance has no flat top (e.g., the center of the acceptance depends on the product of the horizontal and vertical angles leaving the target). (3) Multiple scattering at the entrance to the spectrometer in $S3$, $C4$, and $C5$, the vacuum window, and air also effectively blurs the shape of the acceptance curve. This latter process, which may be considered as an effective enlargement of the target spot as seen by the spectrometer, was particularly important for this experiment, since the enlargement is momentum dependent. No significant dependence of the shape of the acceptance curve on the $\Delta p/p$ in the spectrometer could be found, however, for a given central momentum.

It is clear that as the central momentum in the spectrometer is reduced from 355 to 100 MeV/c in this experiment, increased multiple scattering at the spectrometer's entrance will reduce the effective solid angle. A number of methods were used to measure this effect, but before describing them, it should be pointed out that the results are coupled with the effective target spot size and thus target geometry, with the cuts applied in the trajectory analysis and with the pion-decay correction. Therefore, it was necessary to consider all these aspects together, although in practice it was not always easy to be completely consistent in handling them.

1. Pion decay

For each event, the deviation in path length from the central trajectory is known from the chamber

coordinates, permitting a pion-decay correction to be applied to each event. The possible errors in this are the following: (1) that the trajectory length assumed for the central momentum is wrong (maximum likely error ±50 cm), and (2) that the value used for the dispersion of the spectrometer is wrong, leading to errors in the pion path length calculated for off-central momenta.

Since the overall normalization of the data is derived from π^+-p scattering, an error in the assumed central trajectory length is only of significance in that it will contribute to a momentum dependence of the effective spectrometer solid angle, which is discussed in the next section. An error in the dispersion assumed for this correction would result in inconsistencies in the relative normalizations of overlapping runs. This is discussed in Sec. III F.

2. *Multiple scattering*

Since multiple scattering varies as $1/p\beta$, where p is momentum and β is velocity, we start by pointing out that this begins to increase very quickly for pions below 60 MeV. The principal method of ascertaining the momentum dependence of the solid angle was by measuring the relative normalization of the π^+-p peak in the data. Drawbacks to this technique are that the lowest energy of pions scattered from hydrogen was 55 MeV, that there is a correlation between pion energy and scattering angle (and hence target geometry), and that it is difficult to isolate the required effect from others when comparing data from different data sets. To assist in isolating the effect of multiple scattering, a number of comparative measurements were made.

To understand the acceptance at the lowest momenta, a series of transmission runs were taken. For these, an artificially large beam spot was generated with the spectrometer at 0°. The ratio of pions transmitted through the spectrometer to those incident at $S3$ was plotted as a function of target coordinate, to produce an acceptance curve such as shown in Fig. 4. To establish the normalization of this curve, it is necessary to estimate the fractions of muons and pions at the scintillator $S3$; this was done by a Monte Carlo method. Since most muons do not decay, while 75% of 40 MeV pions decay before reaching $S4$, the uncertainty in the beam composition at $S3$ was not negligible. The weakness of the technique is that it relies on an artificial experiment.

The result of these analyses was to parametrize the dependence on target geometry by a correction factor

$$C_t = 1 + 0.4(1 - \cos\theta_{\text{tgt}}) ,$$

and that on momentum by a factor

$$C_p = 1 + 20/p\beta(\pm 10/p\beta) .$$

The algebraic form of both corrections was arbitrary. The error on C_t was absorbed into that of C_p since their derivations are coupled. The error on C_p was assumed to be correlated for all momenta in one spectrum: For each angle the error at the π^+-p elastic peak is zero, and at other energies the error is assumed to be half of the correction. At energies below 60 MeV, additional errors of 2% to 6% were added in quadrature to account for increased uncertainty in C_p. These errors are included in the systematic errors in the results. As a check of our analysis of the spectrometer solid angle, we compared it to results obtained from the π^+-p normalizations obtained during a very accurate π^+-d elastic scattering experiment,[17] which was performed during the same period as this experiment. These normalization runs were taken over a very wide range of angles, target geometries, and energies, and broadly confirmed our analysis.

It should be emphasized that with these corrections, all data at a given incident pion energy were constrained to have the same normalization (excepting 114 MeV at 134°, which was taken under unique conditions). The maximum relative deviation of the measured π^+-p cross section from that calculated from the phase shifts after this procedure is ±4%.

C. Chamber efficiencies

Data from the multiwire proportional chambers were deemed good if they indicated a single trajectory per plane. Events were accepted only when data from planes $X1$, $X4$, $Y4$, $X5$, $Y5$, $X6$, and $X7$ were all good (the X coordinate corresponds to the bend plane); typical efficiencies were 75% for $X1$, 90% for $X6$ and $X7$, and $>95\%$ for the remainder. The overall chamber efficiency was taken to be the fraction of analyzed events with all planes good. This forms a first-order correction applied to the data.

This definition of the chamber efficiency assumes that all triggers are generated by at least one particle passing through all the planes and that any two-particle events are randomly distributed. In practice, the geometrical definition of the trigger was not perfect, and there were a few coincidences causing triggers where the trajectories of the particles (or noise) causing the trigger was even less well defined. Investigation of these effects resulted in the application of second-order corrections for the efficiencies

of the chambers in the spectrometer.

Since these errors in the chamber efficiencies were caused by a spurious excess of "zeros" in the chambers (and not by multiple hits, which are relatively rare), the investigation concentrated on them. Two principal effects were observed: (1) at momentum settings where the π^+-p elastic peak was just out of the acceptance on the high momentum side, the number of zeros in $X6$, and to a lesser extent in $X7$, was notably high, occurring for 10% to 20% more of the triggers than normal; (2) at low momenta, and especially where there was a substantial muon background in the TOF spectrum, there was a similar effect observed in $C4$. Investigation revealed that these effects could clearly be associated with trajectories passing around instead of through the chambers, and, further, that it was possible to determine reliable estimators for a number of these.

The ($C4$-$C5$) spurious inefficiency was sufficiently uncorrelated with that of ($X6$-$X7$) that the problem could be separated into halves. (Incidentally, this is a confirmation of the unimportance of accidental coincidences in the trigger.) For $C4$ and $C5$, which had delay-line readouts, it was possible to establish a reliable criterion that there was no particle in the chamber. Each chamber had two delay lines (for x and y planes), each with two time to digital converters (TDC). It was found that a criterion demanding that three of the four TDC's have no information was a very reliable indicator of "no particle present." Trials of the criterion two out of four, or all four with no information, gave the same result to $\sim 1\%$, except in a few runs where $C4$ was known from other evidence to be losing efficiency.

For $X6$ and $X7$, which had individual wire readout, there was not a similarly easy criterion to use. However, for a given data set (i.e., data taken at one angle, consecutively), a very good first approximation is that the fraction of true zeros is constant. The most important confirmation of this was provided by comparing the runs near one end of the momentum range measured, but which were taken at the beginning or at the end (chronologically) of that set. Generally, there was good confirmation of the constancy of the chamber efficiency to 1% to 2%, with the exception of the 240-MeV, 110° data, where a steady improvement in efficiency occurred (totalling a 7% change); since this was the only case, it was possible to account for the change without excessive uncertainty.

As a small modification to the correction deduced above, it was determined that the $X6$ and $X7$ had a small but systematic momentum-dependent variation in efficiency. This was deduced by constraining the accepted triggers to a sample in which the geometrical constraints were found to be adequate to ensure that a particle passed through the chamber, and determining the $X6$ and $X7$ efficiencies as a function of momentum for all data sets. The variation found was 5% for momenta from 100 to 300 MeV/c (with higher efficiency for low-energy pions which have higher specific ionization). The total second-order corrections to the chamber efficiencies was usually $< 10\%$ (at most 20%) and an error of one fifth of the correction was assigned.

A further possible source of error is that the 2-m-long focal plane chambers $C6$ and $C7$ could have an efficiency which varied over their length, an effect which is not possible to estimate accurately. However, since a single point in the energy-loss spectrum corresponded to a region > 50 cm in length on $X6$ and $X7$, any variations would be gradual. Minor variations are possible, but searches for effects and consideration of the overall efficiency of $\sim 90\%$ indicate that any variation was under 10%. Furthermore, these variations would tend to cancel when overlapping runs are combined, and so no error is attributed specifically to this source.

D. Dispersion

An error in the value of the spectrometer's momentum dispersion is carried through to a double differential cross section [cf., Eq. (1)], and is not automatically normalized by comparison with the single differential π^+-p cross section $d\sigma/d\Omega$.

By looking at the position of peaks (π^+-p elastic scattering, π^+-^{16}O elastic scattering, and scattering to inelastic discrete states) in overlapping runs, it was possible to determine the dispersion with great accuracy. There was no apparent variation with the experimental condition, and the dispersion was determined to an accuracy of $\pm 2\%$.

E. Incident beam

The incident beam intensity varied from 2 to 5×10^6 π/s, and was usually steady for a given incident momentum. With the 50-MHz beam structure at SIN, this implies an undercounting of the incident beam by 1% to 5%, because of the frequency with which two pions arrived in a single 1-ns-wide beam burst. In general, this error is accounted for by the π^+-p normalization of the data, but corrections of up to 3% were applied to individual runs with anomalously low fluxes. The correction was based on a Poisson statistical analysis of the average pion flux during the run. The validity of this analysis was verified during a high-rate run.

F. Overlapping runs

After applying all corrections to the raw data, a final consistency check was provided by comparing the cross section determined by different, overlapping runs. In general, the agreement was good, but close examination revealed that introducing a correction that varied linearly by $\pm 3\%$ over the full $\pm 10\%$ $\Delta p/p$ acceptance of the spectrometer provided a systematic improvement to the agreement between overlaps. The origin of this effect was not understood—it could not be a dispersion error and it is too big to be associated with a wrong pion-decay correction or its variation with Δp, but could possibly be a true variation of the solid angle. Since applying the small correction clearly improved the internal consistency of the data, and in first approximation did not change the bulk of the final results (where two runs with opposite signs of correction are typically averaged to form each data point), it was applied to all data.

After all corrections, the internal consistency of the data may be quantified by saying that the ratios of the cross sections from all of the overlapping runs were distributed approximately as a Gaussian with $\sigma \sim 4.5\%$. This variance was approximately 1.5 times that expected from the statistical accuracy alone. No significant correlation with incident or scattered pion energy scattering angle, or proximity to the π^+-p elastic peak, was discerned.

G. Energy scale

The incident pion momentum was determined from the magnetic field of the first dipole magnet ($D1$ in Fig. 1), corrected for energy loss in the beam-line detectors and half the target thickness. The scattered pion momentum was similarly determined using the spectrometer's field. The corrections for energy loss were applied to each run individually (using the appropriate material and target thickness), with the dE/dx appropriate to the individual pion.

Thus, the energy scales of the results are corrected to the target-center conditions for both incident and scattered pions. Discrepancies between individual runs, and between the position of the π-^{16}O elastic peak and that expected from kinematics, were usually small and always $<0.3\%$ in momentum.

H. Combination of runs: binning

The data in individual runs were first divided into bins of fixed momentum width, chosen to give a ΔE of <2 MeV generally, but <1 MeV in the regions with significant structure (within 30 MeV of the π^+-^{16}O elastic peak). Data points from different runs were then combined if they were closer than 2 (or 1) MeV, with a weight appropriate to the total error ascribed to the points (i.e., statistical error plus any systematic error assigned to that run from, e.g., the chamber-efficiency uncertainty).

Three of the corrections applied to the data were made on the combined spectra rather than on individual runs; these were corrections for the momentum dependence of the spectrometer's solid angle (see Sec. III B), for the inadequacy of the trajectory analysis (see Sec. III A), and for the finite target thickness (see Sec. III J).

I. π^+-p normalization

The overall normalizations were determined at each angle, as has been stated, by comparing the measured π^+-p elastic scattering data with the phase-shift predictions.[16] The final data, comprising the consolidation of all overlapping runs, were used while individual runs were examined as a consistency check.

It was important to match overlapping runs properly first, in particular by using the correct dispersion, in order not to produce distortions in the resulting peak area. For example, a 5% dispersion error causes peak shifts between different runs, and the nature of the data is such that this produces a change in peak area of a similar amount by artificially broadening or narrowing the resulting peak. In contrast, the area of the peak contained in an individual run is unchanged by varying the dispersion.

J. Finite target thickness corrections

With the target thicknesses used, the attenuation of the beam and the probability of a pion undergoing two interactions were not negligible. Interactions leading to pion absorption or charge exchange reduce both the measured oxygen inelastic and the normalizing π^+-p elastic cross sections equally. Double interactions, such as two inelastic scatterings, or two π^+-p elastic scatterings, or one of each, effectively attenuate the pion flux for the π^+-p scattering, but do not for the continuum oxygen inelastic measurements. Since the π^+ remains in existence, it will in general appear somewhere in the inelastic spectrum at a different angle and at a lower energy than if it had only undergone one scattering. Two π^+-p scatterings thus appear as a background in the inelastic oxygen spectra.

These contributions to the measured spectra were determined by numerical calculation of the probabilities for single and double scattering. The π^+-p cross sections were taken from the phase shifts; the

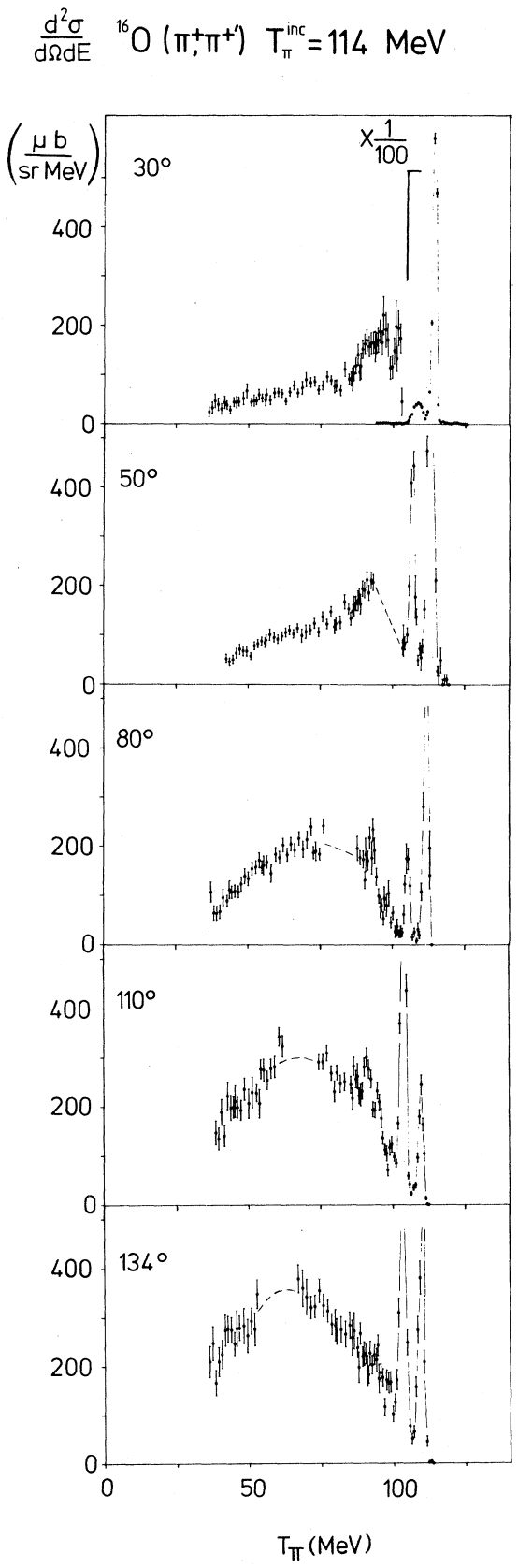

FIG. 5. Double differential cross section, $d^2\sigma/d\Omega\,dE$, for the scattering of 114 MeV pions from ^{16}O, for outgoing pion momenta down to 110 MeV/c, at five scattering angles. At 134°, the data at excitations greater than 10 MeV were taken with poor resolution (target in reflection geometry).

oxygen inelastic cross sections from these measurements with appropriate interpolations and extrapolations in angle and energy. The π^+-^{16}O elastic scattering probability was included, but the differences if it was omitted were small. The attenuations of the incident and scattered beams were determined from the integrals of the differential cross sections used, evaluated at the appropriate pion energies.

The measured spectra were then corrected by (1) renormalizing according to the estimated attenuation loss for the π^+-p peak (-4% to -7%) and (2) correcting the oxygen inelastic spectra both for the estimated absorption loss and for the estimated gain from double interactions (net effects: -3% to 12%). A systematic error of 30% of the net correction was attributed to this source. The effect of these corrections can be broadly summarized as being within a few percent of an overall normalization change (consistent in magnitude with simple estimates), except at forward angles and low energies where the cross sections were reduced by up to a further 10%.

K. Errors

The overall normalization uncertainty is estimated to be $\pm 5\%$ for all spectra. The errors on the individual data points are composed of systematic errors (arising from the three corrections applied to the combined data, see Sec. III H) which are correlated between the points, and "statistical" errors, which are substantially uncorrelated (small correlated errors on individual runs have been included here). The error on the incident momentum scale is $\pm 0.3\%$ and that on the scattered pion's energy scale is $< \pm 1$ MeV.

IV. RESULTS

A. The energy spectra

The double differential cross sections are shown in Figs. 5–7; the error bars on the individual data points in the figures include a contribution from correlated systematic errors, i.e., they are the "total error," excluding only the overall normalization uncertainty of $\pm 5\%$. The incident energy is that at the target center. The angular acceptance was 10°. Tabulated data are available from PAPS.[18] In Figs. 5–7 the large peak from π^+-p elastic scattering

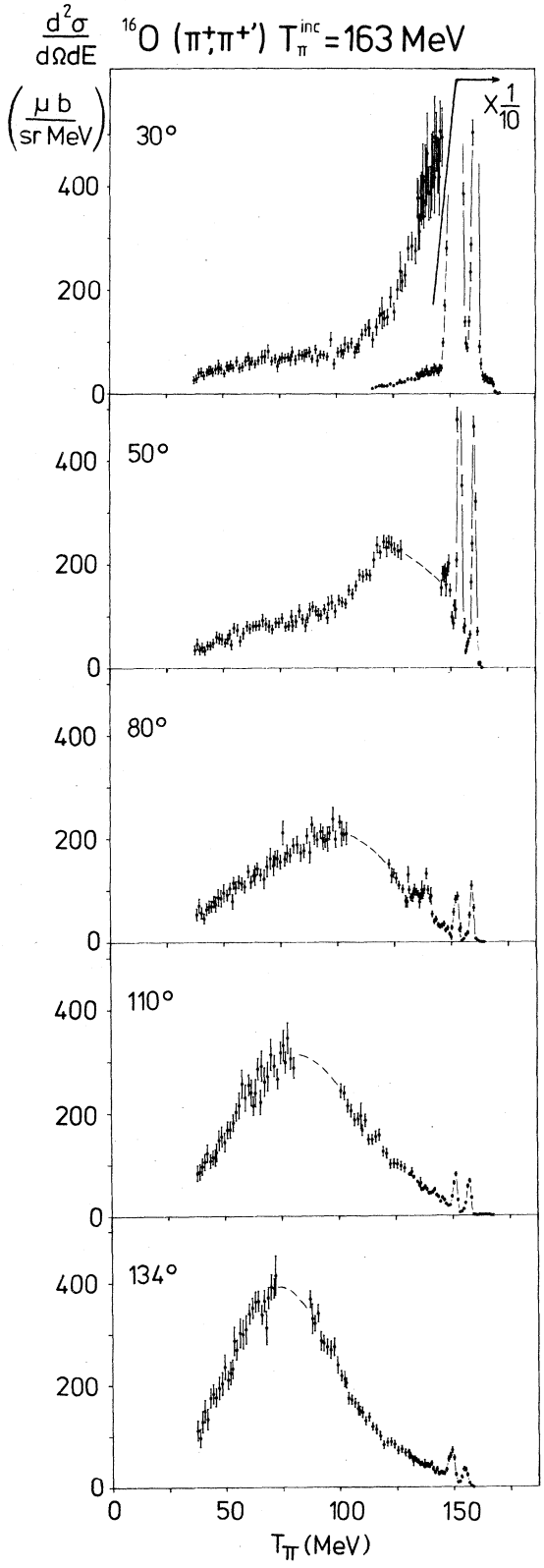

FIG. 6. As Fig. 5, but for 163 MeV incident pions.

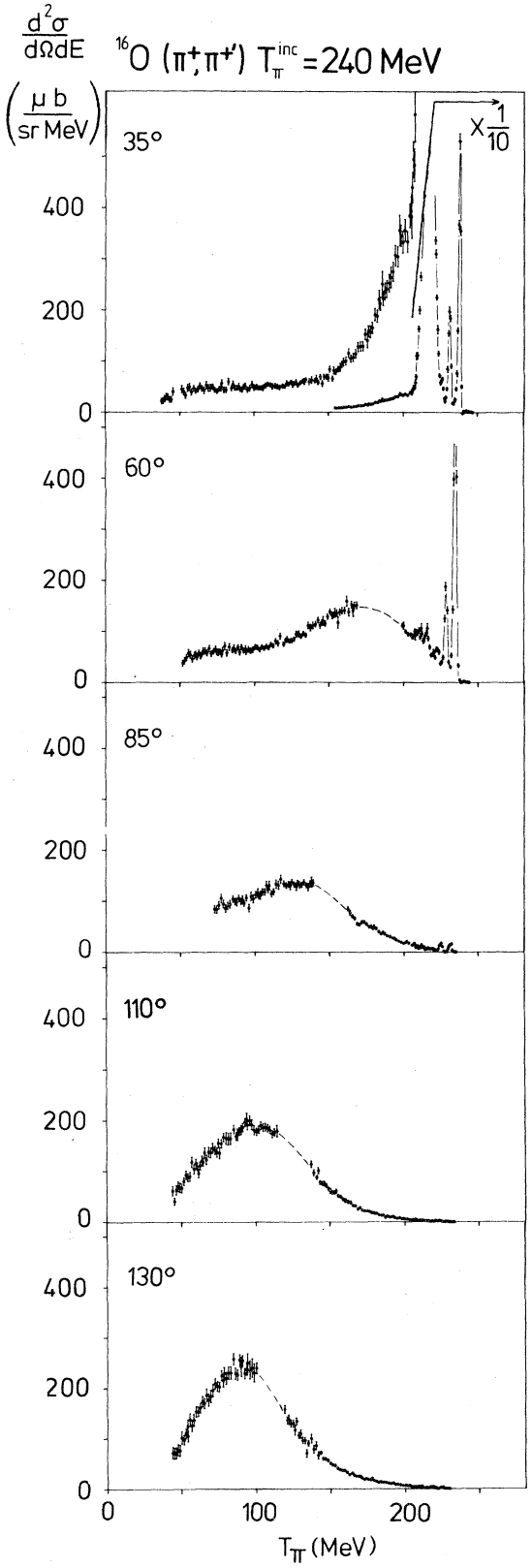

FIG. 7. As Fig. 5, but for 240 MeV incident pions.

from the hydrogen in the water target is not shown except at the most forward angle in each figure, and the resulting gap in the π^+-^{16}O data has been filled by a dashed line to guide the eye.

1. *Dominance of single quasifree scattering*

The principal feature of the data at all incident pion energies and angles is the broad peak in the ^{16}O(π,π') energy spectrum. The position and width of this peak establish that it arises substantially from quasifree pion-nucleon scattering, that is, the single scattering of the pion from a quasifree nucleon in the nucleus.

For such quasifree scattering, the energy loss of the pion is similar to that in free pion-nucleon scattering, modified by the binding energy and Fermi motion of the struck nucleon. It can be seen in Figs. 5–7 that the position of the broad π^+-^{16}O peak follows that from free π^+-p scattering, although with some variations in the relative position, a detail that we shall return to later.

The width of a quasifree scattering peak due to Fermi motion may be expected to be about[19]

$$\Delta E \sim \sqrt{2} q \frac{k_F}{M} , \tag{2}$$

where k_F is the nuclear Fermi momentum ($\sim$220 MeV/c), M the nucleon mass, and q the momentum transfer of the pion. For the scattering of 163-MeV pions to 80°, where $q \simeq 300$ MeV/c, Eq. (2) gives $\Delta E \sim 100$ MeV FWHM. Equation (2) is only a rough guide but shows that the widths of the peaks are of the correct order of magnitude. Phase space is neglected in this estimate, and since the width is comparable to the incident pion energy, the peaks extend towards the threshold regions causing a narrowing as compared to Eq. (2). Comparison of the data with full calculations of quasifree scattering, made later in this paper, confirms that the broad peak is from quasifree scattering.

As a further illustration that the peak has the correct form for quasifree scattering, the data for 240-MeV incident pions scattered at 60° are compared, in Fig. 8, to electron scattering data[20] at the same incident momentum and scattering angle, but on ^{12}C. The electron data have been arbitrarily normalized to match the quasifree peaks. Since the pion is very relativistic, the kinematics of the (π,π') and (e,e') reactions are very similar except at large energy losses where the extra kinetic energy of the incident electron becomes significant. The electron and pion spectra in the region of the quasifree peak are remarkably similar, both in the position and the width of the peak. The weakness of the electron interaction guarantees that the inelastic spectrum below the π-production threshold is dominated by the single quasifree scattering peak. This confirms our interpretation of the peak in the pion data, even though the pion interaction at these energies is, in contrast, extremely strong, and in addition very energy dependent.

2. *Contributions from multiple scattering*

Because of the strength of the pion-nucleon interaction, it is not a trivial point that a single-scattering quasifree peak is clearly visible. The mean free path of a pion in a nucleus, $\lambda = (\sigma_{\pi N} \cdot \rho_N)^{-1}$, is 0.5 to 1 F ($\sigma_{\pi N}$ is the πN total cross section and ρ_N the nucleon density) so that multiple pion collisions must be very likely. In a

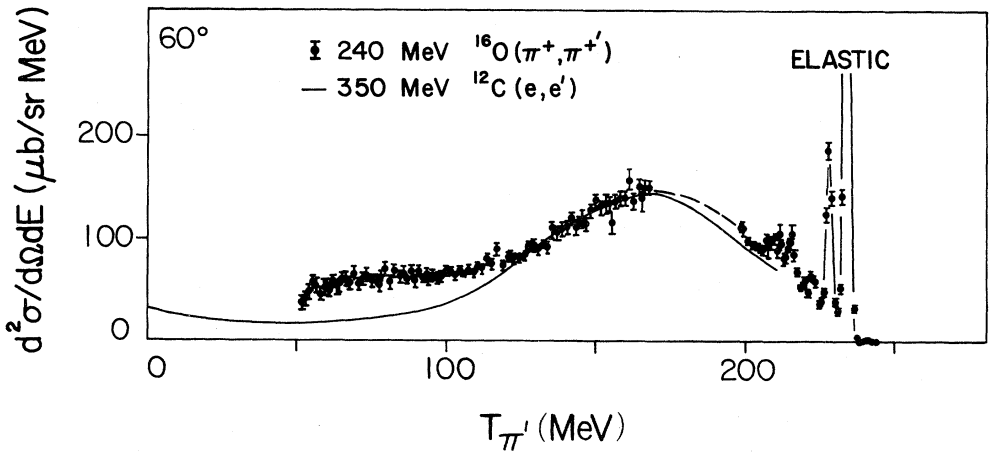

FIG. 8. Comparison of the 240 MeV (353 MeV/c), 60° data of the experiment with the 350 MeV ^{12}C(e,e') data at the same angle of Ref. 20. The normalization of the electron data has been adjusted to match the pion data.

single πN collision the pion loses, on the average, nearly half its incident kinetic energy, and so after two such collisions we might expect its final energy to be around one-fourth of its initial value. After two or more quasifree collisions with nucleons that have a Fermi momentum comparable to the momentum transfer of the interaction, such a pion may be expected to have little correlation between its outgoing angle and final energy. Pions from multiple-interaction processes then should appear near the low-energy end of the spectra of Figs. 5–7 and with a relatively isotropic distribution. Because of the very strong interaction, we might naively expect the spectra to have substantial amounts of these low-energy pions, either dominating the spectra or at least obscuring the single quasifree scattering peak.

At backward scattering angles the energy loss of a pion in a single quasifree interaction is so large that the Fermi-broadened peak approaches the end point ($T_{\pi'}=0$ MeV) and thus there is no clear kinematic separation of pions from single and multiple interactions. However, at forward angles, where the single-scattering quasifree peak occurs at fairly small pion energy loss, there is a clear kinematic separation of the single- and multiple-scattering processes. Thus the sizes of the low-energy tails in the forward-angle data provide useful upper limits to the contributions to the reaction from multiple-scattering processes, and it can be seen from Figs. 5–7 that this yield is actually rather weak, in contradiction to the naive suggestion of the previous paragraph.

The comparison with the electron scattering data of Fig. 8 might be used to determine the multiple-scattering contribution to the 240-MeV data fairly directly by subtraction. However, at large energy loss the pion becomes increasingly less relativistic, so that the two reactions's kinematics diverge and the electron spectrum begins to contain contributions from electropion production. This latter process causes the electron cross section to rise again at energy losses greater than 200 MeV, while the lower incident pion energy precludes any significant contribution from the $(\pi,2\pi)$ reaction.[21] Thus subtraction of the (renormalized) electron data from the pion spectrum gives a minimum estimate of the multiple-scattering yield in the latter. We note in passing that the region of the electron spectrum between the quasifree peak and the rise due to resonant pion production is not well understood.[20]

Another way to estimate the relative importance of multiple-scattering contributions to the $(\pi^+,\pi^{+'})$ reaction uses the inclusive pion double-charge-exchange (DCX) reaction. DCX must involve at least two nucleons, and the simplest mechanism is two sequential quasifree π-N SCX reactions. Double differential DCX (π^+,π^-) cross sections on ^{16}O have been measured at 240 MeV at three angles[21]; the cross sections peak around $T_{\pi'}\simeq 50$ MeV and are fairly isotropic in both magnitude and spectrum shape. In Ref. 21 it was shown that the shape of the DCX spectrum approximates the difference between the $(\pi^+,\pi^{+'})$ spectrum at 60° and estimates of its single-scattering component based on the electron

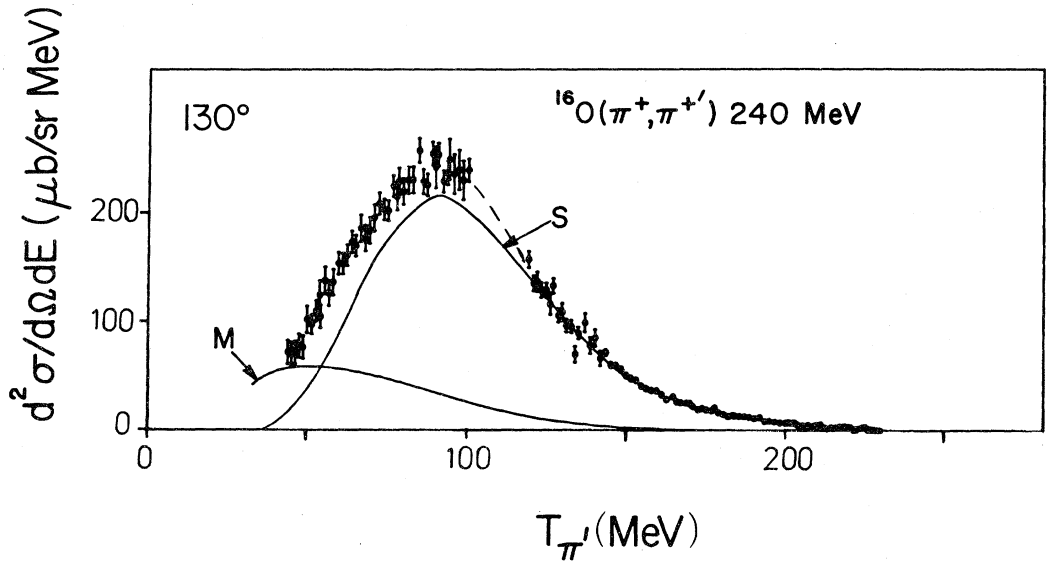

FIG. 9. The 240 MeV data at 130° decomposed to show the contributions from single (S) and multiple (M) scattering as indicated by the DCX data of Ref. 21. The shape of the line labeled "M" is determined from the DCX data at the same angle, with normalization as described in the text. The line labeled "S" is the difference between line "M" and the data.

spectra and calculation.

Since the DCX spectra conform to the expected distribution of pions from multiple-interaction processes, we may assume that they are a fair representation of the distribution in angle and energy loss of the yield from multiple pion interactions in the $(\pi^+,\pi^{+\prime})$ cross section. Using this assumption for the yield's distribution, and normalizing it to the $(\pi^+,\pi^{+\prime})$ cross section at 60° and $T_{\pi'}=60$ MeV, we estimate that about one quarter of the total $(\pi^+,\pi^{+\prime})$ cross section at 240 MeV arises from multiple-scattering processes, with a roughly isotropic differential cross section of some 5 mb/sr. Thus we are able to illustrate, in Fig. 9, a decomposition of the 130° spectrum into single- and multiple-scattering contributions (this is an angle where there is no kinematic separation of the components).

At the lower energies, 163 and 114 MeV, there are no published DCX data, but very recent results[22] indicate that multiple-scattering processes get relatively weaker as the incident pion energy declines. At these lower energies the kinematics for pion and electron scattering become increasingly different, so that direct comparison with electron scattering spectra becomes difficult. However, 200-MeV electron scattering (212 MeV/c corresponds to 114 MeV for pions) from ^{9}Be at 60° (Ref. 23) and from ^{12}C at 80° (Ref. 24) contain significant low-energy tails in their spectra, which cannot arise from either multiple scattering or pion production. This emphasizes that the low-energy tails in the forward-angle pion spectra at 114 and 163 MeV should be taken as indicative of upper limits to the contributions from multiple-scattering processes; these are thus seen to be small compared to the single-scattering peak (Figs. 5 and 6). We will consider this further in Sec. IV A 5.

3. *Sensitivity to the reaction dynamics: multiple scattering*

Our discussion of the spectra so far has shown that although the pion-nucleon interaction implies a very short mean free path for the pion in the nucleus, the inelastic cross section is dominated by single pion interactions. While geometrical arguments may be used to show that there will always be a significant single-scattering yield (from a surface interaction when the pion immediately scatters out of the nucleus), there are clearly mechanisms acting to reduce the multiple-scattering contributions to the spectra, which we will now discuss.

At the energies of this experiment, pions have an incident momentum not much larger than the nucleon Fermi momentum. This has the consequence that some interactions are suppressed by Pauli blocking: The momentum transfer to the nucleon may be inadequate to eject it from the nuclear Fermi sea. After one quasifree collision, the pion typically loses 100 MeV/c of momentum, so that it is harder to eject a second nucleon from the Fermi sea. Thus Pauli blocking must always be more important for a second interaction and especially in the case of the already low momentum 114-MeV incident pions.

The energy dependence of the pion-nucleon cross section is such that for 163- and 114-MeV incident pions, the interaction strength is reduced after the pion loses energy in its first collision. Again this is most important as a mechanism reducing the multiple-scattering probability for the 114-MeV incident pions, since the interaction remains fairly strong until below 100 MeV. For 240-MeV pions, this argument is invalid as the second interaction will frequently be with a higher free π-N cross section.

Pion absorption is a competitive reaction channel, forming 36% of the reaction cross section at 163 MeV (Sec. IV B). When a pion is absorbed, it is irrevocably lost from the (π,π') channel, and so this probability must reduce the total inelastic cross section. However, since the probability of absorption must increase with the number of pion-nucleon interactions within the nucleus, it will also act as a preferential suppressor of multiple-scattering contributions to the inelastic spectrum. The SCX channel also acts in a similar way to remove strength from $(\pi^+,\pi^{+\prime})$ channel with a probability increasing with the number of interactions. The SCX cross section is, however, smaller than that for absorption.

As an illustration of the effects of a competitive reaction channel, it is interesting to consider the situation in inelastic proton scattering where the elementary interaction is also fairly strong. For 90-MeV protons the (p,p') spectra do not show a clear quasifree peak, the low-energy yield being rather large.[25] In this case there is not generally a clear distinction between knockout protons and the incident projectile, and this multiplicity of final state protons helps to obscure the single quasifree peak. There is no strong mechanism analogous to pion absorption to eliminate protons which undergo multiple interactions. At 800 MeV—1 GeV,[26] however, the situation is different and similar to that for pions in a way that emphasizes the role of absorption in pion reactions.[12] At forward angles the quasifree peak of scattered protons is kinematically well separated from the knocked-out nucleons, and now there is also a strong mechanism in Δ production that helps to leave a clear single-scattering peak: The inelasticity of a $p+N\rightarrow\Delta+N$ interaction is large enough to remove those protons well away from the single-scattering peak. The probability of

having produced a Δ increases with the number of interactions, so that the relative yield from double quasielastic scattering processes is weakened and thus these protons do not obscure the single-scattering peak either. In quasifree pion scattering, absorption is a similar strongly competitive channel which removes the pions (in this case entirely from the inelastic spectrum) and which must also make the double pion-scattering yield relatively weak.

It is not possible to distinguish quantitatively the relative importance of the mechanisms we have discussed in reducing the multiple-scattering yield of inelastic pions, and without calculations it is not easy to establish which is most important in a qualitative sense. All nuclear-medium modifications of the pion interaction must be considered, since they affect both the single- and multiple-scattering yields. But pion absorption and Pauli blocking are two explicitly observable medium effects which must quench the multiple-scattering yield, and the size of the absorption cross section indicates the importance of that process. Thus the weakness of the multiple-scattering yield is a feature of the spectra which emphasizes the significance of nuclear-medium effects in the dynamics of the pion-nucleus interaction.

4. *Sensitivity to the reaction dynamics: single scattering*

As noted above, the mechanisms we have cited which affect the multiple-scattering yield will also affect the single quasifree scattering cross section. The effects of medium corrections to the elementary pion-nucleon interaction are best illustrated in comparison with calculations (Sec. IV A 5), except for those due to Pauli blocking which are clear in the angular distributions (Sec. IV B), while the energy dependence of the elementary cross section has qualitatively visible consequences that we shall now discuss.

In Sec. IV A 1, we mentioned that the position of the quasifree peak relative to the free π^+-p scattering peak varied to some extent. Figure 10 shows the most backward angle spectrum at each energy, with the positions of the free π-p peaks and the $^{16}O(\pi,\pi')$ peak centroids (located by eye) explicitly marked. It can be seen that the $^{16}O(\pi,\pi')$ centroid moves systematically relative to the free π-p peak from smaller to larger energy loss as the incident pion energy increases or, more pertinently, as it passes across the resonance. Consider first the 240-MeV data of Fig. 10 in the region where the scattered pion has lost less energy than it does in a collision with a stationary nucleon (indicated by the position of the free π-p peak), i.e., for $T_{\pi'} > 120$ MeV. Pions from single quasifree collisions will fall into this kinematical region if the momentum vector of the struck nucleon is towards the incoming pion. In this case the total center-of-mass energy of the π-N system is greater than that in a free π-N collision. For 240-MeV pions, the free π-N cross section is already well down from the resonance peak, which is at 180 MeV, and increasing the total energy of the π-N collision reduces it further. Thus the quasifree cross section in this part of the spectrum should be depressed by the energy dependence of the π-N interaction. For scattered pions on the other side of the free π-p peak ($T_{\pi'} < 120$ MeV), the kinematical situation is reversed. The π-N collision is closer to resonance and the quasifree cross section is

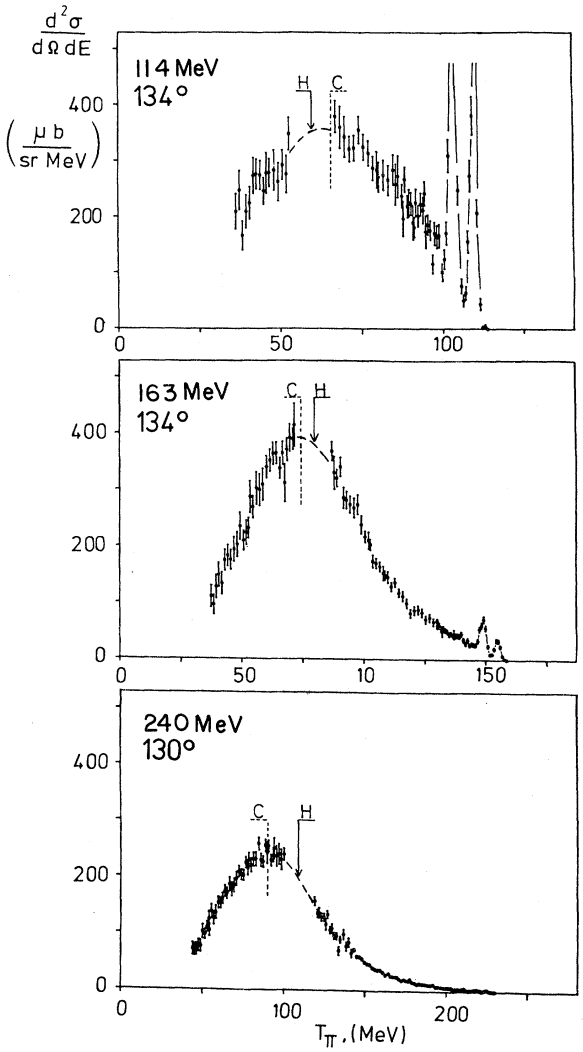

FIG. 10. The double differential cross section at the most backward angle measured for each of the three incident energies. The centroid of the peak in the data, located by eye, is noted (C), and the position of the peak from π^+-p scattering is also marked (H).

enhanced. The relevant change in the π-N total center-of-mass energy, W, over the peak of the 240-MeV spectrum in Fig. 10 is given approximately by

$$\Delta W = 2p_\pi p_F / W \simeq 120 \text{ MeV} ,$$

where p_π and p_F are the momentum of the incident pion and the Fermi momentum of the struck nucleon, respectively. The free π-N cross section changes by a factor of 5 over this energy range.

For 114-MeV incident pions the kinematic situation is analogous, but since the energy is below the resonance, the effect on the cross sections is the reverse: the scattering of pions with large energy loss is depressed and that of those with small energy loss is enhanced.

The shift in the position of the ^{16}O(π,π') peak relative to that of free π-p scattering as the incident pion energy crosses the resonance, as indicated in Fig. 10, may be seen as a consequence of these enhancements and depressions of the cross sections. The shapes, in particular the curvatures, of the quasifree peaks may also be noted. Including the effects of multiple-scattering, backgrounds under the peaks shift the peak positions, but do not alter the interpretation. This is clear from Fig. 9 which shows the decomposition at 240 MeV, where the multiple-scattering contribution is the largest.

It was pointed out in Ref. 7 that these qualitative features of the backward-angle data illustrate the sensitivity of these cross sections to the microscopic (pion-nucleon) interaction dynamics, and so provide a test of pion-nucleus interaction models. In particular, in models which use the fixed-scatterer approximation, there is no recoil of the nucleon or of the Δ, so that there is no change in the effective pion-nucleon interaction energy across the quasifree peak. With no Δ recoil there can be no Δ-nucleus interaction, and so formalisms that do not reproduce this shift in the peak are not only failing to handle the interaction dynamics correctly, but also explicitly exclude the possibility of exploring the Δ-nucleus interaction.

5. *Comparison with theory*

We have explained that the shape of the quasifree scattering peak reflects the strong energy dependence of the pion-nucleon cross section, and have used the weakness of the multiple-scattering yield as an illustration of the importance of nuclear-medium effects. The inelastic pion spectra should, therefore, be a useful test of how well models of the pion-nucleus interaction describe the microscopic interaction dynamics within the nucleus. In the Introduction we pointed out that the strong coupling between the pion and the Δ-hole states in the nucleus implies that a satisfactory description of the pion-nucleon interaction within the nucleus must also include a description of the effects of the nucleus on the recoiling Δ. While the energy dependence of the pion-nucleon interaction may be substantially included on a microscopic basis by a proper evaluation of the kinematics of the collision, nuclear medium modifications of the interaction must be included in a more explicitly model dependent way. Since the pion-absorption probability is strongly energy dependent, and since the momentum of the recoiling Δ formed in the pion collision varies from 0 to 600 MeV/c depending on the kinematics of that collision, we may expect that there is also some importance to having these medium modifications included on a dynamical basis.

Currently, microscopic calculations of the inelastic spectrum in the continuum which describe the intranuclear processes coherently are restricted to the contributions from single quasifree scattering, owing to the complexity of including multistep processes. In such a calculation, it is convenient to separate the elementary interaction, described with an amplitude containing the effects of the nuclear medium, from distortions of the incoming and outgoing pion waves. The calculation must determine the correct, medium-modified pion-nucleon interaction and employ a consistent optical potential to evaluate the distortions. While the separation of the distortion of the pion waves from the medium modifications to the elementary interaction is artificial, since that interaction is the source of the distortions, this separation also allows us to illustrate that these inelastic cross sections depend on the pion-nucleus dynamics over a large energy range. For example, for 240 MeV incident pions scattered to 130°, the quasifree peak extends down to about 50 MeV so that the cross sections are dependent not only on the dynamics of the interaction at its particular kinematics, but also, via the distortions, on the pion-nucleus interaction over the full energy range of the $\Delta(1232)$ resonance.

Calculations of the pion spectra from single scattering using the Δ-hole formalism have recently been published.[27] In this model the nuclear-medium modifications to the pion-nucleon interaction are characterized as interactions of the recoiling Δ formed in the interaction. This Δ-nucleus interaction is described by a simple optical potential whose parameters are determined phenomenologically by fitting the pion-nuclear total and elastic scattering cross sections. Pion absorption is associated in a natural way with the imaginary part of this potential. Pauli-blocking corrections and nonresonant π-N interactions are included, and in this calculation the Δ-nucleus interaction includes a spin-orbit term.

The incoming and outgoing pion waves are distorted by a potential based on the same transition operator used to describe the quasifree collision, and distortion of the knocked-out nucleon wave is also included. All these distortions are found to affect the results of the calculations significantly, varying both the shape and strength of the quasifree peak. Calculations of the quasifree scattering in this model have no free parameters. We show a few examples of the results in Fig. 11 (full lines), compared to our data. The agreement of the calculations with the data is impressive. Deviations of the calculations from the data may be noted at low outgoing pion energies (especially at forward angles) where the multiple-scattering yield is strongest. Nuclear excitations in the 20 MeV region are also poorly described by the nuclear model used. Since the spectra are dominated by single quasifree scattering, these deficiencies do not prevent useful comparison.

At the backward angles the qualitative effect of the shift of the peak position relative to that of the free cross section as the incident energy crosses the resonance is reproduced by the full Δ-hole calculation. The dashed lines in Fig. 11 represent a calculation where there is no Δ recoil and where medium corrections such as pion absorption are excluded. In this case the shift of the peak position is not reproduced, reflecting the incorrect determination of the kinematics of the interaction. For this closure calculation, the absolute magnitude of the cross section is also very poorly determined, especially for the 114-MeV case; Thies[27] states that for the 114- and

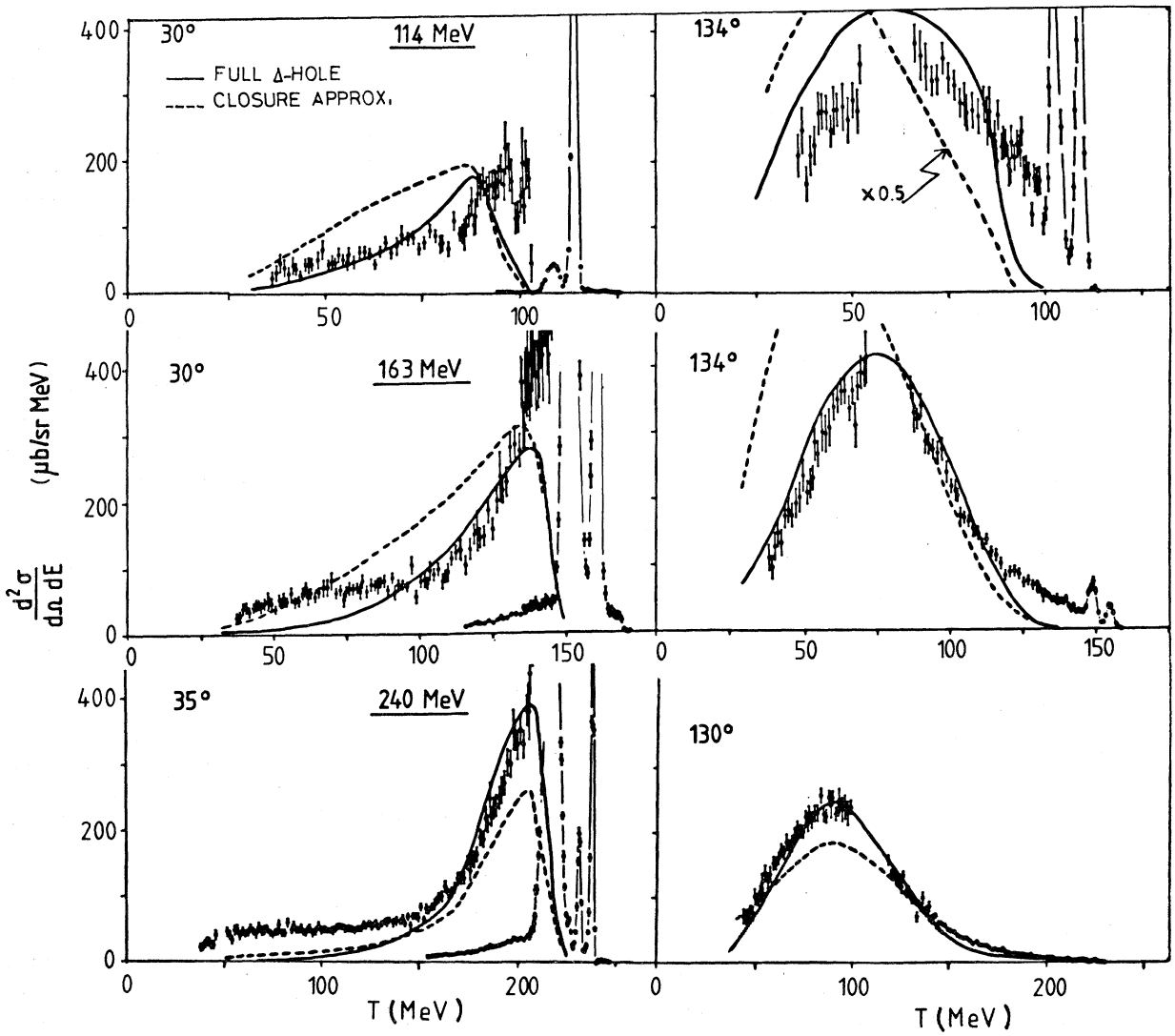

FIG. 11. Comparison of the present results with calculations of Ref. 27 of single quasifree scattering using the Δ-hole formalism. The solid lines are the results of the full calculations; the dashed lines use the closure approximation (see text).

163-MeV cases the overestimation of the cross section in this approximation is due to the failure to reflect a weakening of the transition operator because of medium corrections to the free amplitude, and also to much too weak distortion of the outgoing pion waves below 100 MeV, where the very important inelasticity of the pion-absorption cross section has been neglected. The pion-nuclear total cross section at low energies is also very poorly reproduced in this approximation. For the 240-MeV case, Thies states that the underestimation of the cross section is essentially due to too strong distortion of the outgoing pion wave in the 100–200 MeV region, a reflection of the overestimation of the strength of the underlying pion-nuclear interaction within the nucleus in this energy range. The reader is referred to Ref. 27 for a fuller discussion of these points, but the comparisons of the two calculations with the data confirm the importance of medium effects on the inelastic cross section, and the sensitivity of these results to the pion-nuclear interaction dynamics over a large energy range.

As we have noted, the calculations shown in Fig. 11 should predict too little cross section to the extent of the multiple-scattering yield in the spectra. In the 240 MeV, 35° case, where the multiple-scattering yield in the low outgoing energy region is kinematically well separated from the quasifree single-scattering peak, the deficiency is clear and substantial. There is also a clear, if smaller, deficiency at low energies in the 163 MeV, 30° case, while at 114 MeV, 30°, any discrepancy in the low-energy region is small. In this last case the low-energy region is still close to the quasifree peak (only 70 MeV/c away at $T_{\pi'}=35$ MeV), and the calculation indicates that a substantial part of the low-energy tail in this spectrum is generated by the high-momentum components in the nuclear wave function. This is consistent with the existence of low-energy tails in the electron-scattering spectra at similar incident momenta (see Sec. IV A 2). At backward angles, the lack of kinematic separation from the single-scattering peak of the multiple-scattering yield means that the calculations may not be usefully employed to estimate that yield (except to show that it is probably not very large). But the forward-angle comparisons are further evidence that while the multiple-scattering contribution to the pion inelastic cross section is significant (but not dominant) at 240 MeV, these processes decline in importance with decreasing incident pion energy.

B. Angular distributions and partial cross sections

Integration of the double differential cross sections,

$$d^2\sigma/(d\Omega_\pi dE_\pi)\ ,$$

of Figs. 5–7 gives the differential cross sections for inelastic scattering. These are presented in Fig. 12 and Table II. The uncertainties in these integrated cross sections include contributions from uncertainties in extrapolating to $T_{\pi'}=0$ MeV and in deter-

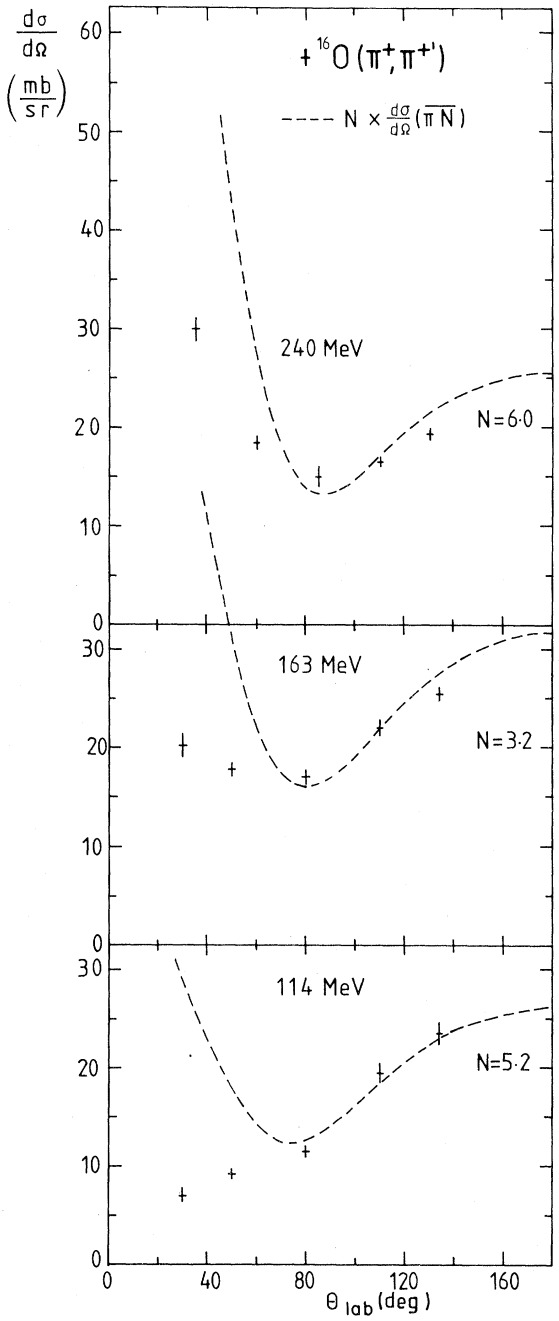

FIG. 12. The inelastic differential cross section, $d\sigma/d\Omega$, as a function of angle for each of the three energies. The dotted line is the average π-N elastic differential cross section multiplied by the factor N.

TABLE II. Differential cross sections for inelastic scattering. The errors exclude the overall normalization uncertainty of ±5%.

Energy (MeV)	Angle (deg)	$d\sigma/d\Omega$ (mb)
114	30	$6.95^{+1.0}_{-0.5}$
	50	9.30±0.65
	80	11.50±0.55
	110	19.5 ±1.1
	134	23.6 ±1.3
163	30	20.2 ±1.2
	50	17.8 ±0.7
	80	17.0 ±0.7
	110	22.0 ±0.9
	134	25.4 ±0.7
240	35	30.0 ±1.2
	60	18.4 ±0.7
	85	15.0 ±1.1
	110	16.50±0.45
	130	19.30±0.55

mining the contribution from excitation of discrete states, but exclude the ±5% normalization error. Figure 13 shows an example of the linear extrapolation to zero pion energy (with the assumed uncertainty) used in the integrations.

At forward angles the dominant discrete states are hidden under the peak from π-p scattering. For the smallest angle at each energy a smooth extrapolation was made to account for the continuum cross section and the contribution of significant discrete states up to 15 MeV of excitation was obtained from a calculation by Holtkamp.[28] In the 114-MeV spectra at 50° and 80° data from BeO and Be targets were available, allowing deduction of the shape of the ^{16}O spectrum below the π^+-p elastic peak. Knowledge of this shape was a significant aid in determining the inelastic cross sections in these two cases.

Since the inelastic cross section is substantially single quasifree scattering, it is reasonable to compare the angular distributions of the integrated inelastic differential cross sections to the average π^+-N differential cross sections. The dotted lines in Fig. 12 represent these π-N cross sections multiplied by a factor N to give agreement at the backward angles. The factor N is seen to vary sharply with incident energy, being smallest at 163 MeV, consistent with the expected maximum distortion of the pion waves near the peak of the π-N total cross section at 180 MeV.

At forward angles the inelastic data fall below the shape of the average free cross section. This may be understood as a consequence of Pauli blocking. At these angles the momentum transfer for quasielastic scattering is comparable to or smaller than the nuclear Fermi momentum, and thus is not always sufficient to eject the nucleon from the Fermi sea. This effect is also clear in the spectra; at backward angles the entire quasifree peak is well clear of the nuclear bound-state region, while at forward angles the small energy-loss side of the quasifree peak is truncated.

While the comparison with the free π-N cross section illustrates these qualitative effects fairly clearly,

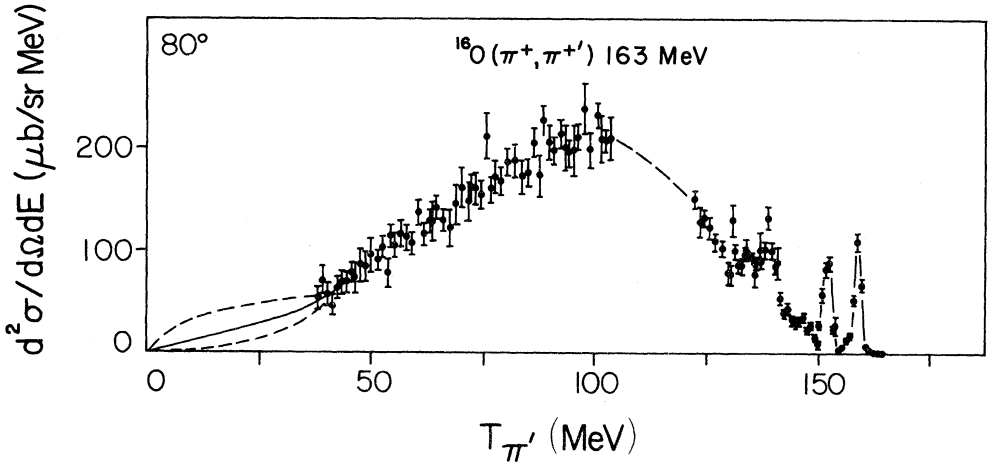

FIG. 13. An example (163 MeV, 80°) of the extrapolation to $T_{\pi'}=0$ MeV employed in the integration of the spectra. The full line is the assumed shape; the dashed lines show the maximum likely deviation. The difference between the full and dashed lines in this case represents an uncertainty of 3.5% in the integral.

a number of additional factors affect the inelastic differential cross sections. These include the relative strength of the almost isotropic multiple-scattering contributions, the energy-dependent (and thus angle-dependent) distortion of the outgoing particle's waves, and finally, the nuclear response function. The integral of this function over the energy-loss spectrum at fixed angle varies with that angle, and this contributes to the rise of the inelastic cross section at backward angles.[29] Thus caution is required in the physical interpretation of N, but it is nevertheless a useful parametrization for comparison of this experiment with other data.

Integration of the inelastic differential cross sections of Table II gives the total inelastic cross sections given in Table III; the errors here include the normalization uncertainty. The results of our partial cross section analysis are also given in Table III. The total cross section[2,3] and the total elastic cross section[15,30] have been measured. We have estimated the total SCX cross section and have thus deduced the total pion-absorption cross section by subtraction. The DCX cross section has also been taken into account at 240 MeV and at the lower energies has been taken to be negligibly small. Other reaction channels, $(\pi,2\pi)$ and radiative channels, are small compared to the error on the deduced absorption cross section.

Our estimate of the SCX cross section was made as follows: At each angle where we have $(\pi^+,\pi^{+'})$ data the (π^+,π^0) cross section was assumed to be equal to the differential $(\pi^+,\pi^{+'})$ cross section at that angle multiplied by the ratio of the free average π-N cross section for the two channels

$$\frac{d\sigma}{d\Omega}[^{16}\mathrm{O}(\pi^+,\pi^0)]=\frac{d\sigma}{d\Omega}[^{16}\mathrm{O}(\pi^+,\pi^{+'})]\frac{\frac{d\sigma}{d\Omega}(\pi^-p\rightarrow\pi^0n)}{\frac{d\sigma}{d\Omega}(\pi^+p)_{\mathrm{el}}+\frac{d\sigma}{d\Omega}(\pi^+n)_{\mathrm{el}}}M\ . \tag{3}$$

An error of 30% was associated with this estimate. The additional factor M represents an estimate of the possible additional multiple-scattering cross section for the SCX channel. Iteration of the $T=\frac{3}{2}$ dominance of π-N total cross sections suggests that double scattering could be 1.75 times more likely than single scattering in the (π^+,π^0) reaction than in the $(\pi^+,\pi^{+'})$ channel. Estimating multiple-scattering contributions to the $(\pi^+,\pi^{+'})$ cross sections at 114, 163, and 240 MeV to be 4%, 10%, and 27%, respectively, gives values for M of 1.03, 1.075, and 1.20. Comparison[31] of (γ,π^+) with $(\pi^+,\pi^{+'})$ spectra at 350 MeV/c justifies belief in a greater contribution from multiple scattering in the SCX channel. In pion photoproduction on free nucleons many more π^0 are produced than π^+ at this energy, and the ^{12}C(γ,π^+) spectrum[32] at forward angles is consistent with secondary pion interactions giving extra π^+ yield from secondary (π^0,π^+) reactions, roughly in accordance with the free cross section ratio estimate.

It may be noted from Table III that while the sum of the nonabsorption inelastic channels contributes a steadily increasing fraction of the total cross section as the energy increases (0.34, 0.40, and 0.47 at 114, 163, and 240 MeV, respectively), the absorption cross section clearly peaks well below resonance, both in absolute magnitude and as a fraction of the total cross section (0.28, 0.23, and 0.13 at the three energies). This weakening of the absorption channel at the higher energies is an important point which must be included both in models of the absorption process itself and in discussion of pion-nucleus dynamics as a whole.

C. Comparison with other experiments

Our results are substantially in agreement with recent related published work. The factor N in Fig.

TABLE III. Partial cross sections for π^+ on ^{16}O.

π^+ energy	114 MeV Cross section (mb)	163 MeV Cross section (mb)	240 MeV Cross section (mb)
σ_{tot}	735±15	807±15	676±15
σ_{el}	280±20	297±20	270±20
$\sigma(\pi,\pi')$	191±12	259±17	249±16
σ_{SCX}	58±17	63±19	62±19
σ_{DCX}			6± 1
σ_{abs}	206±33	188±36	89±35

12, with values of 5.2, 3.2, and 6.0 at 114, 163, and 240 MeV, respectively, can be compared to values of 5.0, 3.0, and 6.0 deduced by interpolation from the results in Ref. 6 (whose N_{eff} must be doubled for an equivalent definition). Ratios of the present inelastic cross sections to those of Ref. 6 are (0.81±0.13), (1.09±0.19), and (1.06±0.19) at the three energies. The overall agreement is satisfactory, although the results of this experiment indicate a slightly different energy dependence. It should be noted that this experiment is a direct measurement of σ_{inel} while the values of Ref. 6 rely on subtraction of partial cross sections. The results at 163 MeV on ^{16}O of Ref. 33 also agree with our results within the quoted errors.

Preliminary spectra for the $(\pi^+,\pi^{+\prime})$ reaction at 146° and 165 MeV on four nuclei, including ^{12}C, have recently been published.[34] These are consistent with our results. The data on ^{12}C at 180 MeV of Ref. 11 appear to be consistent with our cross sections but some results of the older experiments[9,10] on ^{12}C and ^{16}O appear to be wrong. Reference 9 indicates a very rapidly rising total inelastic cross section at 0° below 150 MeV for π^- on ^{12}C, while our results contradict this and indicate that they are roughly a factor 20 too high at 114 MeV. The 270-MeV ^{16}O$(\pi^+,\pi^{+\prime})$ cross section of Ref. 10 at 63° may be somewhat big, but at more forward angles their cross sections rapidly become much too large.

It has been suggested[13] that our preliminary results[7] at 114 MeV were rather low compared to the ^{16}O(π^+,π^0) results[13] at 100 MeV, the ratio of SCX to non-SCX total inelastic cross sections being 1.2 greater than that expected from simple estimates. Even though our final result for the total inelastic cross section $(\pi^+,\pi^{+\prime})$ at 114 MeV is 15% lower than quoted in Ref. 7, we do not find a significant disagreement between the integrated cross sections. Our estimates of the SCX total cross sections extrapolated to 100 MeV give a value of 55±5 mb compared to 66±10 mb in Ref. 13. The error on our estimate includes only that on our cross sections and the extrapolation. We have also extrapolated our value of N to 100 MeV and find agreement (better than 5%), as we do if we extrapolate our estimates of the differential SCX cross sections at 110° and 134° to 100 MeV according to the prescription described in Sec. IV B. On the other hand, the SCX data are relatively large at angles $<90°$, almost following the shape of the free $\pi^-p\to\pi^0n$ differential cross section [i.e., not showing the Pauli blocking effect which is clear in the $(\pi^+,\pi^{+\prime})$ data in Fig. 12]. It has been suggested[7,12] that this may be a consequence of strong final state interactions of the knockout nucleon; the 30° data at 114 MeV in Fig. 5 shows that a good fraction of the cross section leads to bound or virtual states.

It may be noted that our method of estimating the integrated SCX cross section from the $(\pi^+,\pi^{+\prime})$ channel gives a higher $[\text{SCX}/(\pi^+,\pi^{+\prime})]$ ratio at energies below resonance than the method used in Ref. 13, where the total SCX cross section is multiplied by the ratio of free total cross sections

$$[(\pi^+p+\pi^+n)\text{ elastic}/(\pi^-p)\text{ SCX}]$$

to estimate the total ^{16}O$(\pi^+,\pi^{+\prime})$ cross section. Our method similarly uses ratios of free cross sections but takes the differential cross sections to determine the SCX angular distribution [Eq. (3)], which is then integrated to give the total cross section. Since the free SCX cross section is more backward peaked than the free π-N elastic cross section, we would expect Pauli blocking to reduce the total ^{16}O SCX cross section less than the $(\pi^+,\pi^{+\prime})$ cross section because the forward angles contribute a smaller proportion of the total cross section in the SCX channel. Our estimating procedure includes this effect and thus predicts a larger total SCX cross section than a procedure using only total cross sections (by as much as a factor 1.5 at 114 MeV, for instance).

Our estimate of the total SCX cross section being only slightly smaller than the measured value[13] is consistent with the agreement of the two channels at backward angles, where most of the cross section lies. Currently, therefore, the only significant difference between the two channels is at the forward angles. Below resonance multiple pion scattering appears to be very small, so that this is unlikely to produce differences between the two channels, while speculations[31] of large anomalies in the isovector channel are not supported by the current limited amount of SCX data.

V. CONCLUSION

We have shown that inelastic pion scattering from ^{16}O is dominated by single quasifree pion-nucleon interactions for incident energies spanning the Δ(1232) resonance. The contribution to the inelastic cross section from multiple pion-nucleon collisions within the nuclear appears to be small at 114 MeV, but at 240 MeV it is about one quarter of the $(\pi^+,\pi^{+\prime})$ cross section. The partial reaction cross sections show that below resonance the inelastic (including SCX) and pion absorption channels are of comparable magnitude, but that absorption declines in importance rapidly above resonance. The data provide an overview of the inelastic cross section on ^{16}O with sufficient detail to be explicitly sensitive to the interaction dynamics involved. Calculations by Thies[27] in the Δ-hole model successfully reproduce the quasifree cross sections.

Estimates of the yield of pions from multiple quasifree collisions rely heavily on the forward-angle energy spectra where there is good kinematic separation of these pions from those in the single-scattering peak. At 240 MeV comparison with DCX and electron-scattering data and also with the calculations of single-scattering processes provides a convincing identification of the yield from multiple scattering at forward angles. The result that about one quarter of the inelastic cross section of 249 mb at 240 MeV arises from multiple pion collisions follows by assuming the isotropy of this yield, as indicated by the DCX data. While much of the low-energy tail in the forward-angle spectra at 240 MeV clearly comes from multiple-scattering processes, and while there is a noticeable but smaller yield at 163 MeV, the calculations of Thies indicate that much of the low-energy yield in the 114-MeV 30° spectrum may be from single-scattering processes.

The very strong pion-nucleon interaction implies a substantial multiple pion interaction probability, and so other factors must enter to reduce the inelastic pion yield from such processes to the small values observed. We have suggested (Sec. IV A *3*) three such factors: Pauli blocking, the energy dependence of the π-N interaction, and competitive reaction channels, notably pion absorption. We may expect that these factors vary in efficacity with the incident pion energy. The higher the incident momentum, the less important is Pauli blocking. If the incident energy is above resonance, the pion will still have enough energy after one quasifree collision to have a very strong interaction. Finally, the pion-absorption cross section peaks well below resonance, and is relatively small at 240 MeV (Table III). It is not possible to isolate the role of any one of these mechanisms, from each other or from the pion-nuclear dynamics as a whole, but the data we have presented indicate that at 114 MeV they combine to strongly suppress inelastic pions from multiple collisions, while above resonance the mechanisms are weakened, resulting in a significant yield of such pions at 240 MeV. Thus we are able to link qualitative aspects of the results together to form an understanding of the relationship between the various processes occurring in the pion reactions and see how the balance between different parts of the reaction cross section changes across the resonance. We cannot, however, deduce from the data why the absorption cross section should have the strength it does, nor why it declines so fast above resonance.

It is usually considered that inelastic pion scattering is a peripheral process (because of the strength of the interaction) and that pion absorption, which requires the participation of two nucleons, is a more central phenomenon; this is confirmed by the A dependence of the partial cross sections.[6] Our data show that at 240 MeV the cross section for multiple collisions where the pion survives is comparable to that of pion absorption (90 mb). Therefore it is reasonable to expect that, for the less peripheral absorption processes, one or more quasifree interactions before the absorption are more likely than in the case where the pion survives. This implies that the absorption of the pion often occurs at an effective energy well below the incident value (at least if that is over 200 MeV), and this may be confirmed by the large nucleon multiplicities measured in the (π,p) reaction.[8] Therefore the elementary πNN absorption process in nuclei must decline with increasing energy above resonance even more quickly than implied by the π-nucleus total absorption cross section.

The dominance of single quasifree scattering in the inelastic pion spectra facilitates their interpretation and allows comparison with theoretical calculation of that process. The shapes of the spectra and the magnitude of the cross section are sensitive to the interaction dynamics over the entire energy range of the spectra. In the Δ-hole model of Thies the nuclear-medium modifications to the free pion-nucleon interaction are characterized as interactions of the recoiling Δ with the residual nucleus. The Δ-nucleus interaction is described by a complex potential determined phenomenologically from the elastic and total pion-nuclear cross sections. His results show that it is possible to successfully construct a model that acknowledges the special dynamical processes that dominate the pion-nucleus interaction at these energies and therefore may be used as a framework for more detailed study. By demonstrating the strong influence of nuclear-medium effects on the quasielastic channel, the importance of considering medium effects in interpreting other nuclear reactions, where their effect may not be so obviously apparent, is emphasized.

The experiment reported here has furnished data on one nucleus covering a major reaction channel through the $\Delta(1232)$ resonance region, which is sufficiently comprehensive and detailed to provide both qualitative insight into the reaction dynamics and an extensive quantitative test of theoretical models. Similar experiments[34–36] have now been performed over a range of nuclear masses that will provide information on how the balance between single- and multiple-scattering processes and pion absorption depends on the nuclear size and on the neutron excess. Our global understanding of pion-nucleus interactions is now quite good. In order to proceed to a more detailed understanding, where we may learn about the microscopic dynamics of the Δ-nucleus interaction and of pion-absorption processes, extensive

coincidence measurements of quasifree scattering, $(\pi,\pi N)$, and of absorption, (π,NN), are required.

ACKNOWLEDGMENTS

It is a pleasure to thank Dr. F. Lenz for suggesting this experiment and for his continued interest in it, and Dr. M. Thies for many interesting discussions of his calculations. We also thank Prof. E. Moniz and Dr. Y. Horikawa for many useful discussions. Dr. J. Domingo and Dr. K. Gabathuler assisted with the data taking, and Linda Bayliss with the data analysis, for which we are also grateful. One of the authors (J.A.) thanks the Alexander von Humboldt Stiftung for partial financial support. This work was supported by the Schweizerisches Institute für Nuklearforschung, the Bundesministerium für Forschung und Technologie, and the U.S. Department of Energy.

---

*Permanent address: Los Alamos National Laboratory, Los Alamos, NM 87545.

†Present address: Laboratoire National Saturne, F91191 Gif-sur-Yvette, CEDEX, France.

[1]L. S. Kisslinger and W. L. Wang, Ann. Phys. (N.Y.) 99, 374 (1976); K. Klingenbeck, M. Dillig, and M. G. Huber, Phys. Rev. Lett. 41, 387 (1978); E. Oset and W. Weise, Nucl. Phys. A329, 365 (1979); Y. Horikawa, M. Thies, and F. Lenz, *ibid.* A345, 386 (1980).

[2]C. Wilkin, C. R. Cox, J. J. Domingo, K. Gabathuler, E. Pedroni, J. Rohlin, P. Schwaller, and N. W. Tanner, Nucl. Phys. B62, 61 (1973).

[3]N. D. Gabitzsch, G. S. Mutchler, C. R. Fletcher, E. V. Hungerford, L. Coulson, D. Mann, T. Witten, M. Furić, G. C. Phillips, B. Mayes, L. Y. Lee, J. Hudomalj, J. C. Allred, and C. Goodman, Phys. Lett. 47B, 234 (1973).

[4]A. S. Clough, G. K. Turner, B. W. Allardyce, C. J. Batty, D. J. Baugh, W. J. McDonald, R. A. J. Riddle, L. H. Watson, M. E. Cage, G. J. Pyle, and G. T. A. Squier, Nucl. Phys. B76, 15 (1974).

[5]A. S. Carroll, I.-H. Chiang, C. B. Dover, T. F. Kycia, K. K. Li, P. O. Mazur, D. N. Michael, P. M. Mockett, D. C. Rahm, and R. Rubinstein, Phys. Rev. C 14, 635 (1976).

[6]D. Ashery, I. Navon, G. Azuelos, H. K. Walter, H. J. Pfeiffer, and F. W. Schlepütz, Phys. Rev. C 23, 2173 (1981).

[7]C. H. Q. Ingram, *Meson-Nuclear Physics—1979 (Houston)*, Proceedings of the 2nd International Topical Conference on Meson-Nuclear Physics, AIP Conf. Proc. No. 54, edited by E. V. Hungerford III (AIP, New York, 1979), p. 455.

[8]R. D. McKeown, S. J. Sanders, J. P. Schiffer, H. E. Jackson, M. Paul, J. R. Specht, E. J. Stephenson, R. P. Redwine, and R. E. Segel, Phys. Rev. C 24, 211 (1981).

[9]F. Binon, P. Duteil, J. P. Garron, J. Görres, L. Hugon, J. P. Peigneux, C. Schmit, M. Spighel, and J. P. Stroot, Nucl. Phys. B17, 168 (1970); CERN Report PH III-69/19, 1969 (unpublished).

[10]J. Rohlin, S. Rohlin, B. W. Allardyce, J. J. Domingo, C. H. Q. Ingram, N.W. Tanner, E. M. Rimmer, and J. P. Girardeau-Montaut, Nucl. Phys. B37, 461 (1972).

[11]G. R. Burleson, G. S. Blanpied, J. Davis, J. S. McCarthy, R. C. Minehart, C. Goulding, C. L. Morris, H. A. Thiessen, W. B. Cottingame, S. Greene, and C. F. Morre, Phys. Rev. C 21, 1452 (1980).

[12]F. Lenz, Proceedings of the Topical Meeting on Intermediate Energy Physics, Zuoz, 1976, Schweizerisches Institute für Nuklearforschung report, 1976, Vol. 2, p. 319.

[13]T. J. Bowles, D. F. Geesaman, R. J. Holt, H. E. Jackson, J. Julien, R. M. Laszewski, J. R. Specht, E. J. Stephenson, R. P. Redwine, L. L. Rutledge, Jr., E. E. Segel, and M. A. Yates, Phys. Rev. C 23, 439 (1981).

[14]J. P. Albanese, J. Arvieux, E. T. Boschitz, R. Corfu, J. P. Egger, P. Gretillat, C. H. Q. Ingram, C. Lunke, E. Pedroni, C. Perrin, J. Piffaretti, L. Pflug, E. Schwarz, C. Wiedner, and J. Zichy, Nucl. Instrum. Methods 158, 363 (1979).

[15]J. P. Albanese, J. Arvieux, E. T. Boschitz, C. H. Q. Ingram, L. Pflug, C. Wiedner, and J. Zichy, Phys. Lett. 73B, 119 (1978); J. P. Albanese, J. Arvieux, J. Bolger, E. T. Boschitz, C. H. Q. Ingram, J. Jansen, and J. Zichy, Nucl. Phys. A350, 301 (1980).

[16]J. B. Walter and G. A. Rebka, Jr., Los Alamos Report LA-7731-MS, 1979 (unpublished); J. R. Carter, D. V. Bugg, and A. A. Carter, Nucl. Phys. B58, 378 (1973).

[17]K. Gabathuler, J. Domingo, P. Gram, W. Hirt, G. Jones, P. Schwaller, J. Zichy, J. Bolger, Q. Ingram, J. P. Albanese, and J. Arvieux, Nucl. Phys. A350, 253 (1980).

[18]See AIP Document no. PAPS PRVCA-27-1578-23 for 23 pages of tabulated double differential cross section data for $^{16}O(\pi^+,\pi^{+'})$. Order by PAPS number and journal reference from American Institute of Physics, Physics Auxiliary Publication Service, 335 East 45th Street, New York, N.Y. 10017. The price is $1.50 for microfiche, or $5 for photocopies. Airmail additional. Make checks payable to the "American Institute of Physics."

[19]H. Uberall, *Electron Scattering from Complex Nuclei* (Academic, New York, 1971), Sec. 7.2.

[20]J. Mougey, M. Bernheim, D. Royer, D. Tarnowski, S. Turck, P. D. Zimmerman, J. M. Finn, S. Frullani, D. B. Isabelle, G. P. Capitani, E. De Sanctis, and I. Sick, Phys. Rev. Lett. 41, 1645 (1978).

[21]R. E. Mischke, A. Blomberg, P. A. M. Gram, J. Jansen, J. Zichy, J. Bolger, E. Boschitz, C. H. Q. Ingram, and G. Pröbstle, Phys. Rev. Lett. 44, 1197 (1980).

[22]Th. S. Bauer, J. J. Domingo, C. H. Q. Ingram, G. Kyle, G. Smith, and R. Stamminger (private communication); D. A. Clark, P. A. M. Gram, J. L. Matthews, G. A. Rebka, S. A. Wood, and H. J. Ziock (private communication).

[23]H. Nguyen-Ngoc and J. P. Perez-y-Jorba, Phys. Rev. 136, B1036 (1964).

[24]I. S. Gulkarov, N. G. Afanas'ev, A. A. Khomich, V. D. Afanas'ev, V. M. Khvastunov, G. A. Savitskii, and N. G. Shevchenko, Yad. Fiz. 9, 1138 (1969) [Sov. J. Nucl. Phys. 9, 666 (1969)].

[25]B. D. Anderson, A. R. Baldwin, A. M. Kalenda, R. Madey, J. W. Watson, C. C. Chang, H. D. Holmgren, R. W. Koontz, and J. R. Wu, Phys. Rev. Lett. 46, 226 (1981).

[26]D. M. Corley, N. S. Wall, H. Palevsky, J. L. Friedes, R. J. Sutter, G. W. Bennett, W. D. Simpson, G. C. Phillips, G. W. Igo, and R. L. Stearns, Nucl. Phys. A184, 437 (1972); R. E. Chrien, T. J. Krieger, R. J. Sutter, M. May, H. Palevsky, R. L. Stearns, T. Kozlowski, and T. Bauer, Phys. Rev. C 21, 1014 (1980).

[27]M. Thies, Nucl. Phys. A382, 434 (1982).

[28]D. Holtkamp, Los Alamos National Laboratory Report LA-8231-T, 1980 (unpublished).

[29]Y. Horikawa, F. Lenz, and M. Thies (private communication).

[30]M. Hirata, J. Koch, F. Lenz, and E. Moniz, Ann. Phys. (N.Y.) 120, 205 (1979).

[31]C. H. Q. Ingram, Nucl. Phys. A379, 319 (1982).

[32]J. Arends, J. Eyink, H. Hartmann, A. Hegerath, B. Mecking, G. Nöldeke, and H. Rost, Z. Phys. A 305, 205 (1982).

[33]I. Navon, E. Piasetzky, D. Ashery, A. Altman, G. Azuelos, F. W. Schlepütz, and H. K. Walter, Phys. Lett. 95B, 365 (1980).

[34]S. M. Levenson, D. F. Geesaman, E. P. Colton, R. J. Holt, H. E. Jackson, J. P. Schiffer, J. R. Specht, K. E. Stephenson, B. Zeidman, R. E. Segel, P. A. M. Gram, and C. A. Goulding, Phys. Rev. Lett. 47, 479 (1981).

[35]M. Baumgartner, H. P. Gubler, G. R. Plattner, W. D. Ramsay, H. W. Roser, I. Sick, P. Zupranski, J. P. Egger, and M. Thies, Phys. Lett. 112B, 135 (1982).

[36]J. Källne, J. F. Davis, J. S. McCarthy, R. C. Minehart, R. R. Whitney, R. L. Boudrie, J. McClelland, and A. Stetz (unpublished).